Stochastic atmospheric forcing as trigger for sudden Greenland warmings *

Hannah Kleppin † and Markus Jochum

Niels Bohr Institute, University of Copenhagen, Copenhagen, Denmark

Bette Otto-Bliesner

Christine A. Shields

Stephen Yeager

National Center for Atmospheric Research, Boulder, Colorado

*submitted to J. Climate, October 24^{th} 2014

†*Corresponding author address:* Hannah Kleppin, Niels Bohr Institute, University of Copenhagen, Juliane Maries Vej 30, 2100 Copenhagen, Denmark

E-mail: kleppin@nbi.ku.dk

ABSTRACT

An unforced simulation of the Community Climate System Model 4 (CCSM4) is found to have Greenland warming and cooling events that resemble Dansgaard-Oeschger-cycles in pattern and magnitude. With the caveat that only 3 transitions were available to be analyzed, we find that the transitions are triggered by stochastic atmospheric forcing. The atmospheric anomalies change the strength of the subpolar gyre, leading to a change in Labrador sea-ice concentration and meridional heat transport. The changed climate state is maintained over centuries through the feedback between sea-ice and sea-level pressure in the North Atlantic. We discuss indications that the initial atmospheric pressure anomalies are preceded by precipitation anomalies in the West Pacific warm pool. The full evolution of the anomalous climate state depends crucially on the climatic background state.

1. Introduction

Abrupt climate transitions occurring in the North Atlantic (NA) region and in particular at Greenland during the last glacial period, spanning the period from about 120,000 to 12,000 years ago, are well documented in various climate proxy archives, the most frequent ones being Dansgaard-Oeschger cycles (D-O events, Dansgaard et al. (1993)). D-O events feature a distinct pattern of abrupt warming of 8 to 16 $^{\circ}C$ (e.g., Landais and Coauthors (2004), Huber and Coauthors (2006)) followed by gradual cooling of the same amplitude. The cold and warm phases are called stadials and interstadials, respectively. D-O events occur most frequently in Marine Isotope Stage 3 (MIS3) and are also associated with a reorganisation in atmospheric circulation as infered from various dust and deuterium excess measurements of Greenland ice cores (e.g., Steffensen et al. (2008)). The snow accumulation rate during the interstadials is 50-100$\%$ larger then during the stadials (Andersen et al. 2006). DO events coincide with abrupt changes in the tropics and large parts of the northern hemisphere (an overview of paleoclimatic proxies indicating coinciding shifts with Greenland temperature can be found e.g., in Rahmstorf (2002)) and Antarctic changes of opposite sign (Barbante et al. 2006).

Interestingly there is also present day evidence for abrupt warmings at Greenland, although they are smaller in amplitude: around 1920 a warming of about 4$^{\circ}C$ at several meteorological stations at Greenland is reported by Cappelen (2013). The warming lasted over a decade and was followed by a slight cooling until the mid-eighties.

First hypotheses trying to explain D-O events were based on an abrupt shutdown of the Atlantic Meridional Overturning Circulation (AMOC), initiated by fresh water input into the NA (e.g., Broecker et al. (1990)). More recent studies with state-of-the-art climate models revealed that the amount of fresh water necessary to slow down the AMOC sufficiently to produce temperature changes at Greenland comparable to D-O events depends on model details (Kageyama et al. (2013), Manabe and Stouffer (1999), Dijkstra (2007)), as well as on the location of the freshwater forcing (Mignot et al. 2007) and its timing (Bethke et al. 2012). Bethke et al. (2012) demonstrate that different models produce a wide range of outcomes for the deglaciation, given the same forcing. However, there is little unambiguous evidence for AMOC shut down during D-O events. A recent study finds instead that a strong AMOC prevailed during most parts of the last glacial period (Böhm et al. 2015) and shut down of the AMOC occured only during Heinrich events close to LGM. Furthermore, the evidence for freshwater input into the NA during D-O events is still subject to discussion. Based on sea level reconstructions from the Red Sea Arz et al. (2007) suggest up to 25 m global sea level rise at the onset of interstadials. On the other hand Siddall et al. (2003) and Rohling et al. (2008) suggest a higher sea level during stadials.

Some of the more recent hypotheses trying to explain D-O events invoke sea ice - atmosphere interactions. Li et al. (2005) find that a reduction of sea-ice extent can cause a climatic response consistent with D-O signals of temperature and accumulation measured from Greenland ice cores. The authors point out, that in addition to the well known ice-albedo feedback, sea ice strongly influences regional air temperatures by insulating the atmosphere from the ocean heat reservoir. The possibility of “switching the ocean-atmosphere heat exchange off” due to extensive sea ice cover provides a plausible mechanism for abrupt and large local temperature changes, even though the initial forcing might be relatively small. Far-field signals and ocean-atmosphere feedbacks are not represented in their study, due to prescribed sea surface temperatures (SST) and an inactive ocean component. In their study the mechanism causing the displacement of the sea ice edge remains unexplored. Li et al. (2010) extends the previous study by implementing more realistic sea ice retreat scenarios. They find that the displacement of the sea ice edge in the Nordic Seas causes a 10 $°C$ warming and 50 % increase in accumulation at Greenland summit, whereas sea ice changes in the western NA have less effect.

Rasmussen and Thomsen (2004) find a subsurface warming during Greenland stadials from a marine sediment core taken from the Nordic Seas. Based on sediment records Dokken et al. (2013) confirm this subsurface warming and suggest a mechanism that could explain a sudden melt of sea ice and hence in combination with the results of Li et al. (2005) explain reconstructed D-O events. During the stadial phase warm Atlantic inflow is separated from surface and sea ice by a strong halocline, allowing for a large ice cover to persist. The mechanism proposed to initiate the abrupt melting involves a slow subsurface warming during stadials due to the separation of the warm Atlantic inflow from the surface. Eventually this subsurface warming destabilises the water column, the halocline collapses and warm subsurface water is reaching the surface and melting the sea ice.

Studying the climate response to highly idealised scenarios of prescribed external forcing (e.g., freshwater-hosing experiments, prescribing sea ice cover changes) gives insight into the particular process and helps to determine its potential influence on Greenland temperatures. However, the origin of the prescribed external forcing remains unclear. To our knowledge there are only five examples of abrupt climate changes arising spontaneously in coupled climate models, i.e, without been triggered by variations in external forcing. Hall and Stouffer (2001) describe a cooling event around Greenland in a fully coupled climate model with coarse resolution. The event lasts for a period of only 30-40 years and is caused by a persistent northwesterly wind anomaly transporting cold and fresh water into the NA and causing a shutdown of deep water convection. Goosse et al. (2002) describes cooling events occurring in an Earth System Model of Intermediate Complexity (EMICs). The cold events are attributed to a displacement of the oceanic deep water convection sites to a more southern location. Just as in Hall and Stouffer (2001) the shut down of deep water convection is induced by stochastic atmospheric forcing, but in addition Goosse et al. (2002)

demonstrate that such an event could also be triggered by appropriate changes in solar irradiance. The remaining three examples of spontaneous climate transitions occur in state-of-the-art fully coupled climate models. Sidorenko et al. (2014) report several events of sudden decrease of deep water convection and increase of Labrador Sea (LS) ice extent. The mechanism behind it is not studied in detail, but the authors attribute them to anomalously saline and warm water inflow into the deep LS. The anomalous light deep water weakens the subpolar gyre (SPG) circulation causing a change in the upper-LS fresh water budget. The warm and saline bias in the deep NA is mainly attributed to too strong surface winds in the subtropical NA, modifying the path of Gibraltar Strait outflow in the NA. Martin et al. (2014) report about centennial-scale variability of the AMOC and other changes in the NA (as e.g., SPG strength and NA heat content) driven by Southern Ocean deep water convection variability. The signal transmission to the NA occurs through an enhanced meridional density gradient between deep (below 1200 m) NA and South Atlantic and a compensation of Antarctic Bottom Water by increased NA deep water extent. Drijfhout et al. (2013) describe a spontaneous cold event with a duration of about 100 years. The authors attribute the cold event to a period of anomalous high atmospheric blocking above the eastern subpolar gyre. The blocking causes the sea ice edge to progress farther south in the Greenland Sea and eventually excites a cold core high pressure anomaly at the south western tip of Greenland. The anomalous anticyclone advects cold air through enhanced northerly winds to the sea ice edge, causing the sea ice extent to grow even farther. Additional sea ice is transported southwards by ocean currents and causes a fresh surface anomaly in the LS. As a consequence deep water convection shuts off and due to longer exposure of the ocean surface to the atmosphere sea ice growth commences, reinforcing the atmospheric anomaly. The anticyclone itself, once fully developed, causes a change from northerly to more southerly winds, advecting warm air, melting the sea ice and returning the system to normal.

Here, we document three climate transitions occurring in a 1000 year pre-industrial control simulation of the Community Climate System Model 4 (CCSM4). These are two gradual cooling and one abrupt warming event around Greenland. The analysis is focused on the first cooling event. The atmospheric anomaly during the cold event resembles closely the one described by Drijfhout et al. (2013). However, the evolution and hence the cause of the cold NA phase is different. It involves a strong positive feedback loop of the SPG circulation. The first weakening of the SPG is caused by decrease in wind stress curl associated with a stochastic atmospheric circulation anomaly. The decreased gyre circulation changes the salinity transport into the highly sensitive deep water convection site in the LS, thus reducing here the deep water convection and eventually affecting the AMOC. This is followed by a rapid increase of sea ice cover and a drop in Greenland temperature. The increased sea ice cover itself forces a reorganisation of the atmosphere, thus sustaining the anomalous atmospheric forcing of the gyre circulation for about 200 years.

The objective of this paper is to identify processes and regions of atmospheric, oceanic and sea ice interactions that play a key role in the transitions between cold and warm NA phases and to suggest a consistent sequence of atmospheric, oceanic and sea ice interactions. In Section 2 we give a brief overview of CCSM4, the set-up of the control simulation and the different experiments that we carried out. Section 3 comprises the results structured as follows. We describe how the events manifest themselves in Greenland, the NA and globally (Section 3 a), followed by a description of the stochastic atmospheric trigger (Section 3 b 1), the dynamics of the ocean response and sea ice changes (Section 3 b 2) and the atmospheric feedback (Section 3 b 3). The sequence of events leading to the abrupt warming is documented in Section 3 c. Finally we assess the dependence of the proposed mechanism on the particular background climate (Section 3 d) and test the atmospheric trigger in forced ocean simulations (Section 3 e). A possible influence of tropical temperature and precipitation anomalies on NA atmosphere circulation changes is discussed. The paper concludes with a discussion of our main findings in Section 4 and a summary in Section 5.

2. Model

The numerical experiments are performed using CCSM4, which consists of the fully coupled atmosphere, ocean, land and sea ice models. A detailed description of this version can be found in Gent et al. (2011). The ocean component is POP2 and has a horizontal resolution that is constant at 1.125° in longitude and varies in latitude from 0.27° at the equator to approximately 0.7° in high latitudes. In the vertical there are 60 depth levels; the uppermost layer has a thickness of 10 *m*, the deepest layer has a thickness of 250 *m*. The atmospheric component uses a horizontal resolution of $1.9^\circ \times 2.25^\circ$ (longitude and latitude, respectively) with 26 levels in the vertical. The sea ice model shares the same horizontal grid as the ocean model and the land model is on the same horizontal grid as the atmospheric model. This setup constitutes the released version of CCSM4, and further details can be found in Danabasoglu et al. (2012). The subsequent sections will analyze and compare several different simulations listed in Table 1. The simulations are either conducted with the fully coupled version or the ocean-sea ice version with prescribed atmospheric fluxes and river run off. The main focus is on a 1000 year long pre-industrial control simulation (CONT), in which the earth's orbital parameters are set to 1990 values and the atmospheric composition is fixed at its 1850 values (for details of the atmospheric composition see Gent et al. (2011)). For comparison with CONT and as initial conditions for some of the experiments described below we make use of an other pre-industrial control simulation (HI). HI differs from CONT only in the horizontal resolution of the atmospheric component which is $0.98^\circ \times 1.258^\circ$. An overview of differences and similarities between CONT and HI is provided by Shields et al. (2012) and discussed in Section d.

Danabasoglu et al. (2012) and Danabasoglu et al. (2014) assess the fidelity of the CCSM ocean module. For CONT in particular we find that the AMOC is well represented at $26.5°N$ with a maximum of 18.4 Sv at 1000 m, compared to the observed maximum of 18.6 Sv, also at 1000 m (Cunningham et al. 2007). The SPG circulation strength (spatial maximum of about 50 Sv) in CONT agrees fairly well with observations by Johns et al. (1995) and Pickart et al. (2002) of 48 and 40 Sv, respectively.

In a 200 year average previous to the transitions CONT features a cold ($\sim 2°C$) and fresh (0.2 PSU) bias in the upper 100 m of the western SPG and the LS compared to temperature (Locarnini et al. 2010) and salinity (Antonov et al. 2010) data from the World Ocean Atlas 2009 (WOA09). Below the surface the model is too warm and salty by about 1 $°C$ and about 0.3 PSU, respectively. In both, WOA09 and CONT maximum mixed layer depths are during March in the LS with values in excess of 1400 m.

To ensure that the transitions are not caused by any numerical or computational issues several runs branching from CONT were performed to test the reproducibility of the occurring transitions. The branch runs (DO_a-f in Table 1) were started using initial conditions from CONT at different points in time. The initial conditions are modified by a random $\mathscr{O}(\varepsilon)$ perturbation.

The conducted branch runs reproduce the climate transitions (2 warming (DO_c,d) and 3 cooling (DO_a,b and DO_F) transitions) even though the transitions in the branch runs occur at different points in time and not always with the same amplitude as in CONT. The annual maximum sea ice concentration in the LS of the original time series (black) and the branch runs (different colors) are depicted in Figure 1. The reproducibility of the climate transitions gives us trust in our findings beyond the lack of statistical analysis possibility. A 200-year extension (DO_X) of CONT was conducted without any further transitions occurring, thus the second cold phase last at least 400 years. Possible reasons for the lack of transitions in DO_X are discussed in Section 4. This and the occurrence of the branch run transitions at different times suggest that a stochastic process triggers a switch between two co-existing climate states. Furthermore the different durations of the cold phases points to the fact that no particular build up time for any kind of reservoir (e.g., warm subsurface water) is involved.

To test the proposed role of the stochastic atmospheric trigger, we conducted several ocean-ice (OI) simulations with different atmospheric forcings 1). For this purpose a part of CONT was rerun, saving the atmospheric fluxes at 3 hour intervals. The OI experiments were started from HI initial conditions and were forced with annually repeating atmospheric fluxes from DO_F (July to June). The different starting years and the forcing year from DO_F are listed in Table 1. We chose starting years preceding a rapid sea ice increase in DO_F for experiments with transitions from a warm to a cold NA phase (OI_a, OI_b-d). Year 305/306 in DO_F preceds a rapid sea ice decrease and was utilised to reproduce the warming transition (OI_f).

3. Results

a. Sequence of events

The pre-industrial control simulation analyzed here features abrupt surface temperature changes in Greenland and in the whole northern hemisphere. In the entire simulation three transitions between warm and cold NA phases occur (Figure 2, upper panel). The annual mean cooling in Greenland is approximately 3 $°C$ (averaged over Greenland (55 to 15$°W$ and 65 to 80$°N$)) over the course of about 100 years followed by an abrupt warming over a decade. At the south-west coast of Greenland temperature changes are more than three times that value. Cooling and warming are more pronounced during winter months. The global surface temperature signature of the cold NA phase is depicted in Figure 3. The strong warm anomaly off the coast of New Foundland is due to a contraction of the SPG (described in more detail in Section 3 b) and the resulting northward migration of the Gulf Stream. The opposite sign anomalies in the Southern Ocean and parts of Antarctica are small in amplitude (about 0.5 to 1 $^{\circ}C$) compared to the changes around Greenland. This anti-correlation is suggestive of the “bipolar seesaw“ (Stocker and Johnsen 2003), but is not analyzed here because of the small signal-to-noise ratio. The tropical temperature signal of the climate transitions is also small in amplitude compared to the high northern latitude changes, but has the same sign. Tropical Pacific precipitation changes associated with the cold NA phase feature a dipole pattern that corresponds to a precipitation decrease in the western Pacific warm pool (WPWP) and a simultaneous increase in the eastern tropical Pacific. This is consistent with paleo-reconstructions that connect Greenland stadials with decreased precipitation over the WPWP and dominant El Niño-like conditions (Stott et al. (2002), based on magnesium/calcium composition and $\delta^{18}O$ of planctonic foraminifera).

The onset of the events based on Greenland temperature are years 321, 590 and 719 (e.g., Figure 2, black lines). In the following subsection we focus only on the first cooling event (year 321). The sequence of events leading to the abrupt warming (year 590) is briefly documented in Section 3 c. Section 3 b describes the dynamics of the climate transition based on the following sequence of events. A stochastic atmospheric circulation anomaly, resembling a strong negative North Atlantic Oscillation (NAO) phase is forcing a circulation anomaly in the SPG (Section 3 b 1). The SPG switches to a weak circulation mode due to a salinity driven positive feedback loop, shutting down deep water convection in the LS, and weakening the AMOC. Associated with weaker circulation mode is a colder surface subpolar ocean (Section 3 b 2). As a consequence sea ice concentration increases in the LS, which in turn causes a reorganisation of the atmosphere and a drop in Greenland temperature (Section 3 b 3).

The atmospheric changes over the NA can thus be separated into two parts. An initial trigger that resembles a negative NAO phase, weakening of the SPG circulation and an increasing sea ice cover, and a positive sea-ice - sea level pressure feedback , an anticyclonic anomaly that persists for about 200 years, and sustains the anomalous atmospheric forcing of the ocean.

b. Dynamical changes

1) Atmospheric trigger

In the beginning (year 310 to 315, upper left panel in Figure 4) an anticyclonic SLP anomaly evolves, centered between Greenland and north western Europe and resembling a negative NAO phase. The anticyclonic anomaly moves south westward and decays over the next 5 years (upper right). The NAO is known to drive the dominant part of NA - in particular the LS - ocean heat transport variability, through changes in wind stress and buoyancy forcing (e.g., Eden and Willebrand (2001)). The total surface heat flux over the LS weakens at this point by about 14 Wm^{-2} (second column in Table 2) as expected from a negative NAO phase (i.e., less heat loss of the LS to the atmosphere). The surface heat flux over the entire SPG region decreases as well, though the amplitude is small. At about the same time the wind stress curl north of the zero wind-curl line reduces (Figure 5, upper left and right). The maximum changes are located above the central and eastern SPG where they account for a 30 to 50 % reduction compared to the long term mean. Furthermore the zero wind-curl line shifts farther north, contributing to a contraction of the SPG. To estimate the importance of the changed wind stress curl in forcing the anomalous SPG circulation the Sverdrup transport was calculated according to Sverdrup theory (e.g., Pedlosky (1996)). The Sverdrup transport in the LS and the north-western NA (averaged from 53° to 61°N and 59° to 45°W) is compared to the actual circulation changes in this region and the entire SPG (Figure 6). The Sverdrup transport reproduces the mean and the anomalous SPG circulation well.

2) Ocean and sea ice response

The decreased wind stress curl forcing causes a first weakening of the SPG circulation (Figure 6). This weakening initiates a positive feedback loop in the SPG leading to the large ocean temperature (color) and circulation (contours) response depicted in Figure 7. The difference in the strength of the circulation in the core region of the SPG accounts for about 10 Sv, a 30 % reduction. At the southern edge the circulation changes up to 20 Sv due to a northward shift of the Gulf stream path. Panel b of Figure 8 shows the density-depth evolution in the LS. The density in the upper LS starts to decrease immediately after the anomalous gyre circulation sets in due to a drop in salinity of 1.6 *psu* (compare to differences in Figure 9 a and b) The salinity content in the LS changes mainly due to changes in advection (through the southern and eastern face of the box) and diffusion of salt (Table 2). A decrease of salinity is seen in the entire water column of the LS (from 65 $^\circ$ to $55^\circ W$ in Figure 9) but with lower amplitude than at the surface. There is a small warm anomaly (0.1 to 0.3 $^\circ C$) in the LS in the intermediate and deeper ocean during the cold phases. However, the warm anomaly never becomes strong enough to destabilize the water column and thus can not trigger the onset of the warm phase, as described by Dokken et al. (2013) for the Nordic Seas. The intermediate depth warming is more pronounced in lower latitudes (up to 45 $^\circ N$).

The decrease of salinity in the LS and the entire SPG is a direct consequence of the slowdown of the SPG circulation. This can be inferred from the large changes in salinity advection (Table 2) and was previously shown by Born et al. (2013b). The authors show that salt transport in the Irminger current increases with a stronger circulation of the SPG, independent of possible negative salinity anomalies in the source region of the Irminger current. They find that the enhanced volume transport overcompensates possible low salinity anomalies in the source region by about two orders of magnitude. In reverse that implies a decreased salinity transport towards the LS and central parts of the SPG during periods of decreased gyre circulation. While increased salinity advection causes long distance salinity transports from the eastern (more saline) basin of the SPG, the actual convergence of salinity in the LS and thus in the deep water convection area occurs due to subgrid, parameterised processes, i.e., eddy fluxes (Born et al. 2013b).

As a result of the decreased surface density the water column in the LS is stably stratified and deep water convection weakens (upper panel in Figure 8) and eventually shuts down completely. Jochum et al. (2012) also find an increased sea ice cover weakens the SPG circulation through insulating it from wind stress forcing. Slightly increased MLD south of Iceland indicate a minor compensation of deep water formation at this location during the cold phase. This is caused by a warm temperature anomaly at a depth of $\sim 1300\ m$ (not shown). The decrease in deep water convection in the LS causes a slow down of the AMOC (max. AMOC located around a depth of 880 m and between 35° and $40°N$, Figure 8). The reduced horizontal density gradient between the center and the boundary current (Figure 8,b) weaken the gyre circulation further, thus closing the positive feedback loop (Born and Stocker (2014) and Born et al. (2013a)).

The changed surface heat fluxes lead to a cooling of the atmosphere, but imply a warming of the LS. The simulated cooling of the LS is a consequence of reduced convection and advection of temperature (Table 2). In contrast to the LS the heat budget in the SPG-box is dominated by changes in temperature advection, due to a decrease of heat advected into the box through the south and from below, partly balanced by a decrease in heat advected through the north face). Diffusion and surface fluxes counteract the cooling tendency of the decreased advection, but are smaller in magnitude.

As a consequence of the colder ocean temperatures sea ice growth commences in the LS. Annual maximum sea ice concentration, in average, increases here by about 100 % relative to its pre-transition state equivalent to about 30 % increased sea ice concentration (Figure 2, lower panel).

The difference in horizontal extent of annual maximum sea ice concentration between the cold and warm NA phases is depicted in Figure 10. The changes are largest in the LS (up to a difference of 90 % sea ice coverage) and stretch from there with lower amplitude along the south eastern coast of Greenland, north of Iceland towards Svalbard and until the northern coast of Norway. A similar spatial pattern of sea ice increase is observed at the north-eastern coast of Asia (not shown) though smaller in amplitude. The sea ice edge progresses farther south and east in the Nordic Seas, the north Pacific and the LS as indicated by the white and black contours in Figure 10. The transition in LS sea ice concentration takes about 80 years from warm to cold (year 321 and 719) and about 20 years from cold to warm (year 590, compare Figure 2, lower panel). Both sea ice growth and retreat start in the LS region, before spreading to the other regions.

In the Nordic Seas the surface layer is fresher and colder during the cold NA phase. However, the warmer subsurface Atlantic inflow becomes colder and less saline too and a strong halocline is always sustained. Changes in thermohaline structure around Iceland (the Nordic Seas) occur about 10 (30) years after the decrease in Greenland temperature sets in and reflect thus most likely the changed ocean circulation.

3) Atmosphere response

The reduced heat fluxes (about 70 Wm^{-2}, last column in Table 2) above the LS (i.e., cooling of the atmosphere) are mainly a result of increased sea ice cover in the LS. They force a cold core high pressure anomaly, which sustains the anomalous forcing of the weakened gyre circulation. This atmospheric response starts to become apparent from year 320 to 325 onwards (Figure 4, lower left). The anomaly strengthens in amplitude south-west of Greenland above the LS and extends, with reduced amplitude, far above the Asian continent. It persits for about 200 years (lower panel in Figure 4) with an average spatial maximum of 2.8 hPa above the LS. Associated with this is also a persistent decrease in wind stress curl (lower panels Figure 5). The largest changes occur west off Greenland where the wind stress curl reduces to about 70 % of its original magnitude (year 50 to 250) and to about 60 % of its original magnitude above the central part of the SPG.

This response of atmospheric circulation to sea ice anomalies was demonstrated by Deser et al. (2007) on shorter timescales, i.e., over one winter/spring season. This is a directly forced baroclinic response and opposite in sign to the equivalent barotropic response to positive (negative) SST anomalies which is invoked to explain the evolution of negative (positive) NAO-phases (e.g., Farneti and Vallis (2011)). The equivalent barotropic response is fully established after 2-2.5 months (Deser et al. 2007) and dominates the overall response. However, in our case the anomalous ocean forcing of the anticyclonic anomaly persists during the entire cold phase, due to the involved ocean circulation changes.

Eventually the sea ice concentration changes cause the drop in Greenland temperature by insulating the atmosphere from the ocean heat reservoir as suggested by Li et al. (2005) and Li et al. (2010).

Above we identified the key changes associated with the climate transition, here we support the suggested sequence of changes based on a lead-lag correlation of key variables with SPG circulation (Figure 11). Changes in atmospheric parameters associated with the trigger are leading changes in the SPG circulation by about three to five years, that are heat flux changes in the LS (blue), SLP south-east of Greenland (not shown) and the Sverdrup transport (cyan) in the northern SPG and LS region. This time scale is in excellent agreement with the suggested time lag of 3 years after that the SPG strength reduces in response to wind stress curl changes associated with a negative NAO (Eden and Jung 2001). Greenland temperature (black) and sea ice (red) concentration changes occur with a lag of about 5 years. As pointed out previously all changes in the salinity budget occur after changes in the heat budget (Table 2) of the LS and the SPG and are thus not included here.

c. Warming event

For the warming event the timing of the changing parameters becomes less apparent from a correlation analysis and is thus defined in terms of their standard deviation. The SLP anomaly decreases for the first time around year 500 but remains then for an other ~ 50 years in a slightly lower but stable state and decreases continuously from around year 550. The anticyclonic SLP anomaly located at the southern tip of Greenland starts to weaken and simultaneously a cyclonic SLP evolves, centered off northern Norway. From here the cyclonic center moves to the central Arctic Ocean around year 580, slowly displacing the anticyclonic SLP anomaly at the southern tip of Greenland. This SLP anomaly resembles closely the anomaly that evolved beside the anticyclone above Greenland in DO_a,b (green and red curve in Figure 1) and appeared to hinder the full amplitude of changes to evolve in DO_a,b. Finally SLP drops abruptly to its pre-event value between year 595 and 600. The surface heat fluxes in the LS and SPG change around year 580 and 570 respectively, while the Sverdrup transport features to high interannual variability to determine smaller trends previous to a sudden jump back to the pre-cooling state at around year 595. The SPG gyre circulation changes around year 577 and sea ice concentration and Greenland temperature follow at years 580 and 590, respectively. It appears that the warming event starts in the SPG, while the cooling event starts in the LS. However the method used to determine the starting point of the transition is not precise enough to conclude a different mechanism from this, given the short time lags. In general the warming and the cooling event feature the same sequence of events that is atmospheric circulation changes (SLP, surface heat flux and wind stress (only determinable for the cooling transition)) followed by SPG circulation changes and eventually a change in sea ice concentration in the LS followed by changes in Greenland temperature. This raises the question why the transitions, at least in Greenland temperature, feature an asymmetric pattern. This question is not addressed in detail but possible causes are discussed in Section4.

d. Dependence on the climatic background state - a comparison to the HI preindustrial control simulation

The question arises why such climate transitions are hardly simulated by state-of the art GCMs (compare Section1). In the following section we thus address this question in terms of the dependence of the above described mechanism on the climatic background state -in particular the differences of HI and CONT in the NA are compared. Both runs are set up with the same external boundary conditions and only differ in the resolution of the atmosphere. However, the mean states of ocean and atmosphere are different. The following numbers refer to a comparison between the ocean and atmosphere state in the NA in a 50 year average directly previous to the first transition and the same time period in HI. To begin with HI features a warmer SPG (about 0.5° to 2 °) and a more saline western SPG (about 0.3 to 0.6 *psu*) and is slightly less saline in the eastern SPG (about 0.1 *psu*). This difference has already some implications for the proposed positive feedback mechanism in the SPG. The effect of salinity anomalies on the density of water is higher for colder temperatures. Thus in HI higher salinity advection anomalies would be necessary to initiate the described positive feedback loop, including the shut-down of deep water formation in the LS. Moreover the western SPG is already less saline in CONT and thus a smaller salinity advection anomaly can already cause the stabilization of the LS water column. Secondly the circulation in the SPG is weaker in CONT and is thus again in favoring conditions for a switch to a weak circulation mode. Furthermore the atmospheric mean state over the NA is distinctly different in both simulations as Figure 12 reveals. The SLP distribution between Greenland and Iceland shows that the Icelandic low is more pronounced in HI, that is a lower mean SLP of about 2 *hPa*. A smaller SLP anomaly in CONT thus weakens the Icelandic low sufficiently to trigger the above described ocean circulation changes. Compared to NCEP reanalysis data (Kalnay et al. 1996) from 1948 until 2014, HI seems to overestimate and CONT to underestimate the Icelandic low (HI and CONT are pre-industrial control simulations). However, the spread of both distributions seems to be realistic. As we hope to infer from the above described abrupt climate transitions about glacial millenial scale variability the SLP distribution of the same region is compared to the one from a LGM simulation (simulation described by Brady et al. (2013)). During the LGM the Icelandic low is distinctly weaker than even in CONT. Lastly CONT features stronger ENSO variability than HI and present-day observations (Shields et al. (2012) Fig. 17).

e. Ocean-sea ice experiments with anomalous atmospheric forcing - testing the trigger

To test the above proposed mechanism and to infer more details about the atmospheric circulation anomaly and the relative importance of buoyancy and wind stress forcing of the SPG circulation anomaly, several OI simulations are conducted (Section 2). In Figure 13 the annual maximum sea ice concentration in the LS is depicted as an indicator of the climate transitions. OI_b-d and OI_a feature rapid increasing sea ice concentration (red, magenta, red with crosses and green with crosses). OI_e,f show a decrease in sea ice concentration (black and black with crosses) where the later one was started from ocean sea ice conditions of the red curve experiment (i.e., from a high sea ice concentration state).

For the longest experiment (red curve, OI_b) the circulation change of the SPG and the MLD in the LS between the 5 first and last years of the simulation were compared. The MLD in the LS decreases by about 240 *m* and the circulation changes in the core region of the SPG account for about

6 *Sv* - a value similar to the 10 *Sv* in CONT. Thus the experiments seem not only to reproduce the changes in sea ice concentration, but as well the ocean circulation changes.

4. Discussion

Based on the scenario above, three topics deserve further attention:

1. Stochastic forcing
2. Tropical-extratropical atmospheric connections
3. Dependence on background climate state

1) Stochastic forcing

We tested the proposed mechanism by forcing OI-experiments with atmospheric fluxes extracted from CONT and starting from ocean and sea ice conditions of HI. That these simulations reproduce not only the same changing sea ice concentration but also the same changes in ocean circulation gives us confidence in the aforementioned mechanism. This sensitivity to stochastic forcing raises the question of what forces the SPG in the real world? Unfortunately there is still no consensus, as reflected in ongoing discussions on whether buoyancy (e.g., Yeager and Danabasoglu (2014) and Eden and Jung (2001)) or wind forcing (e.g., Eden and Willebrand (2001), Häkkinen et al. (2011)) dominates the strength of the SPG circulation. This depends as well on the considered timescales, with a faster response time to altered wind stress forcing.
Altered atmospheric circulation during the last glacial period is expected due to changed ice sheets - in particular the Laurentide ice sheet. This presence causes principal rearrangements in the steady atmospheric circulation pattern above the NA and could thus also explain the absence of D-O events during the Holocene (compare e.g., Wunsch (2006)). A recent study by Zhang et al. (2014) demonstrates that small variations in height of the Laurentide Ice sheet can cause

a shift between two co-existing glacial ocean circulation regimes. They find that this is due to a positive ocean-atmosphere-sea ice feedback similar to the one described herein. We showed additionally that the distribution of SLP above the NA in CONT is biased towards the state of a LGM simulation of the same model, compared to present day observational values and HI.

Furthermore there is evidence from observations that atmospheric rearrangements occur previous to Greenland temperature changes. Steffensen et al. (2008) find by analysing deuterium excess that Greenland precipitation sources change 1-3 years before Greenland air temperature. Change of moisture source region implies an abrupt change of the local atmospheric circulation or the opening of a new source (by e.g., changing from sea ice covered to open ocean). Both changes are seen in CONT: we find atmospheric rearrangements over the NA previous to the abrupt temperature change. In addition the sea ice cover changes in the LS lead the temperature signal and thus establishing/removing a possible Greenland precipitation source.

An interesting aspect of the atmospheric forcing is that it might contribute to the sawtooth-shape of the Greenland temperature signal. Deser et al. (2004) and Deser et al. (2007) find that the amplitude of the SLP anomaly forced by anomalous sea ice cover (or SSTs) is nonlinear in respect to the sign of the anomaly, i.e., decreased sea ice concentration (or warmer SSTs) cause a cyclonic anomaly stronger in amplitude than the anticyclonic anomaly forced by increased sea ice concentration (colder SSTs). Thus larger changes in sea ice cover and temperature are necessary to build up the anticyclonic anomaly than decreasing it again by increasing temperatures and decreasing sea ice cover.

2) Tropical- extratropical connections

The initial change in SLP is in the range of natural variability, thus no further trigger is needed to explain the stochastic atmospheric anomaly over the NA to occur. However, Sardeshmukh et al. (2000) and Palmer (1993) showed that unlike the mean of pressure distribution in the extratropics, the probability of extreme events is strongly influenced by El Niño Southern Oscillation (ENSO) variability. Therefore in the following section we discuss changes in temperature and precipitation in the tropical Pacific and possible connections with the anomalous NA atmospheric circulation. For all three transitions (warm to cool: year 321 and 719; cool to warm: first changes at year 550, finally back to initial state around year 590) changes in tropical precipitation occur simultaneously or previous to the changes in SLP over the NA (Figure 14). Teleconnections from tropics to extratropics work virtually instantaneous, whereas a signal transferred inversely takes about two to three years (Chiang and Bitz 2005). Two other strong increases in precipitation at around year 350 and 890 are both followed by a weakening of the anticyclone and a temporary drop in sea ice concentration (compare to Figure 2). Furthermore temperatures in the WPWP are anomalously warm for about 20 to 30 years previously to the two cooling events. The shifts in tropical atmospheric deep convection associated with SST changes generate planetary waves that change global patterns of SLP (e.g., Sardeshmukh and Hoskins (1988)). It is difficult to associate unambiguously particular sea level pressure changes with particular convection changes (Ting and Sardeshmukh 1993), but the present SLP differences between cold and warm NA phases are quite similar to pressure differences induced by El Niño teleconnections (e.g., Trenberth et al. (1998)): in particular a weakening of the pressure difference between the Azores and Iceland. A modelling study by Merkel et al. (2010) shows altered ENSO teleconnections during past glacial climates. They demonstrate that teleconnections into the NA were strong during pre-industrial times (not shown, but also true for CONT) and Greenland interstadials, while there were weak or no teleconnections during the LGM, Heinrich stadial 1 and Greenland stadials (Figure 11 in Merkel et al. (2010)). Furthermore different ENSO variability is expected with different orbital forcing as also demonstrated by a modelling study of Timmermann et al. (2007). Paleo-reconstructions showed that ENSO was at work over past glacial climates (e.g., Tudhope and Coauthors (2001)). Whether the strength was weaker, stronger or not altered at all during past glacial climates is still debated. Whether the suggested tropical changes are a plausible scenario for D-O events depends thus upon better paleo-reconstructions of altered ENSO strength and variability and its relative timing to Greenland ice cores.

3) Dependence on background climate state

As mentioned previously, no further transitions between NA cold and warm phases occur in a 200 year extension of this simulation, meaning that the last cold state last for at least 400 years. This points towards a strong dependence on the climatic background state for the full chain of aforementioned processes to evolve. The analyzed simulation has a warm bias in global average, but a cold bias in the NA and drifts towards a colder state. The ocean loses heat at -0.09 Wm^{-2} over the last 600 years (Shields et al. 2012). Furthermore the NA (20° -70°N) becomes more saline at intermediate depth while the upper NA ($\leq$ 500 m) becomes less saline, which has a stabilising effect for the cold phase as stronger salinity anomalies are necessary for deep water convection to resume. We discussed in Section 3 d the differences between HI and CONT and how these differences promote the positive feedback loop in SPG circulation, salinity advection and deep water convection intensity as well as the probability of the triggering SLP anomaly to occur. CONT represents in several aspects a climate that is biased towards a glacial climate (e.g., temperature of the SPG, SLP distribution above the NA (compare to Figure 12)).

The reproducibility of the transitions together with the fact that they occur at different points in time compared to the original simulation indicate that no long term memory effects are necessary for the abrupt transitions to occur. Hence it supports our hypothesis that rather quasi-stochastic atmospheric forcing triggers a switch in a per se unstable ocean circulation regime, the strong and weak SPG circulation modes. It would be thus very interesting to analyze a parameter space (mainly of temperature and salinity) for which the SPG can flip. Born and Stocker (2014) show that a simple 4-box model of the SPG is bistable. However, in reality and in a fully coupled climate model the parameter space would be more complex (i.e., ocean-atmosphere and ocean-sea ice feedbacks). How representative this simple model is for the real SPG remains unclear, but for our argumentation it is sufficient that the SPG is sensitive to small perturbations.

5. Summary

D-O-like events are found in a free CCSM4 integration and analyzed. The climate transitions are triggered by a stochastic change in SLP pattern over the NA. This state is associated with a weakened wind stress curl over the SPG. Consequently the gyre circulation slows down and advects less warm and saline subtropical waters to high latitudes, initiating a positive feedback loop towards a persistent weaker state of the SPG circulation and deepwater convection in the LS. Sea ice growth commences in the LS due to locally reduced warm water transport and decreased ocean-atmosphere heat flux. The sea ice anomaly here allows for a cold core high to develop at the south-western tip of Greenland and sustains the anomalous SLP pattern for about 200 years, the entire cool NA phase. The decreased deep water convection leads furthermore to a reduced AMOC of about 3 to 4 Sv and thus a further reduction in northward heat transport. The onset of the warming is initiated by a stronger Icelandic low and thus by removing the anomalous atmospheric forcing the SPG circulation recovers, deep water convection resumes, sea ice cover retreats and Greenland temperature rises abruptly. The possible influence of tropical precipitation anomalies on the NA atmospheric trigger is discussed.

The present coupling between SPG, sea-ice and Icelandic low has already been hypothesized by Seager and Battisti (2007). The central role of the sea ice has already been discussed by Li et al. (2005), though the mechanism causing a sudden sea ice retreat remains unclear. We have now identified a cause for sea ice changes: stochastic atmospheric forcing. The initial trigger of the transitions occurring herein and in Drijfhout et al. (2013) are in both cases stochastic atmospheric circulation anomalies, additionally the anomalous state of the atmosphere during the cold event are alike. However the mechanisms sustaining this persistent anomaly are different. While Drijfhout et al. (2013) attributes the persistent anomaly to sea ice-atmosphere interactions later on amplified by ocean circulation feedbacks (mostly AMOC), we find that the changed oceanic gyre circulation plays a key role. Even though we see changes in thermohaline properties in the Nordic Seas and the LS we find no evidence for the mechanism suggested by Dokken et al. (2013).

The present results are a promising starting point into the dynamics behind D-O events. To us it appears that their most critical and uncertain component is their sensitivity to the NA background state and the structure of atmospheric noise that is needed to trigger a switch in the SPG state. Thus, we plan to continue our work with three complementary approaches: Firstly, find observational constraints for the MIS3 period; secondly, perform more idealized GCM studies in which we can control background state and atmospheric noise; and thirdly, set up a full MIS3 simulation with CESM.

Acknowledgments. We are grateful to Matthew Long and Keith Lindsay for helping setup the ocean-ice simulations. Further we thank Andreas Born and Gokhan Danabasoglu for their insightful comments. We would like to thank Sybren Drijfhout and two anonymous reviewers for the constructive comments that helped to significantly improve this study. NCEP Reanalysis data are provided by the NOAA/OAR/ESRL PSD, Boulder, Colorado, USA, from their Web site at http://www.esrl.noaa.gov/psd/. Computing resources were provided by the Climate Simulation Laboratory at NCAR's Computational and Information Systems Laboratory, sponsored by the National Science Foundation and other agencies

References

Andersen, K. K., and Coauthors, 2006: The Greenland ice core chronology 2005, 15–42ka. Part 1: Constructing the time scale. *Quaternary Science Reviews*, **25 (23)**, 3246–3257.

Antonov, J., and Coauthors, 2010: World Ocean Atlas 2009, Volume 2: Salinity. S. Levitus, Ed. *NOAA Atlas NESDIS*, **69**.

Arz, H. W., F. Lamy, A. Ganopolski, N. Nowaczyk, and J. Pätzold, 2007: Dominant Northern Hemisphere climate control over millennial-scale glacial sea-level variability. *Quaternary Science Reviews*, **26 (3)**, 312–321.

Barbante, C., and Coauthors, 2006: One-to-one coupling of glacial climate variability in Greenland and Antarctica. *Nature*, **444 (7116)**, 195–198.

Bethke, I., C. Li, and K. H. Nisancioglu, 2012: Can we use ice sheet reconstructions to constrain meltwater for deglacial simulations? *Paleoceanography*, **27 (2)**.

Böhm, E., and Coauthors, 2015: Strong and deep Atlantic meridional overturning circulation during the last glacial cycle. *Nature*, **517 (7532)**, 73–76.

Born, A., and T. F. Stocker, 2014: Two stable equilibria of the Atlantic subpolar gyre. *J. Phys. Oceanogr.*, **44 (1)**, 246–264.

Born, A., T. F. Stocker, C. C. Raible, and A. Levermann, 2013a: Is the Atlantic subpolar gyre bistable in comprehensive coupled climate models? *Clim. Dynam.*, **40**, 2993–3007, doi:10.1007/s00382-012-1525-7.

Born, A., T. F. Stocker, and A. B. Sandø, 2013b: Coupling of eastern and western subpolar North Atlantic: Salt transport in the Irminger Current. *Ocean Science Discussions*, **10 (2)**, 555–579, doi:10.5194/osd-10-555-2013, [http://www.ocean-sci-discuss.net/10/555/2013/].

Brady, E. C., B. L. Otto-Bliesner, J. E. Kay, and N. Rosenbloom, 2013: Sensitivity to glacial forcing in the CCSM4. *J. Climate*, **26 (6)**, 1901–1925, doi:10.1175/JCLI-D-11-00416.1.

Broecker, W. S., G. Bond, M. Klas, G. Bonani, and W. Wolfli, 1990: A salt oscillator in the glacial Atlantic? 1. The concept. *Paleoceanography*, **5 (4)**, 469–477.

Cappelen, J., 2013: Greenland-DMI historical climate data collection 1873-2012 - with Danish abstracts. *DMI Technical Report 13-04. Copenhagen*, [http://www.dmi.dk/laer-om/generelt/dmi-publikationer/2013/].

Chiang, J. C. H., and C. M. Bitz, 2005: Influence of high latitude ice cover on the marine Intertropical Convergence Zone. *Clim. Dynam.*, **25 (5)**, 477–496, doi:10.1007/s00382-005-0040-5.

Cunningham, S. A., and Coauthors, 2007: Temporal variability of the Atlantic meridional overturning circulation at 26.5 N. *Science*, **317 (5840)**, 935–938.

Danabasoglu, G., S. C. Bates, B. P. Briegleb, S. R. Jayne, M. Jochum, W. G. Large, S. Peacock, and S. G. Yeager, 2012: The CCSM4 ocean component. *J. Climate*, **25 (5)**, 1361–1389, doi:10.1175/JCLI-D-11-00091.1.

Danabasoglu, G., and Coauthors, 2014: North Atlantic simulations in coordinated ocean-ice reference experiments phase ii (CORE-II). Part I: Mean states. *Ocean Modelling*, **73**, 76–107.

Dansgaard, W., and Coauthors, 1993: Evidence for general instability of past climate from a 250-kyr ice-core record. *Nature*, **364 (6434)**, 218–220.

Deser, C., G. Magnusdottir, R. Saravanan, and A. Phillips, 2004: The effects of North Atlantic SST and sea ice anomalies on the winter circulation in CCM3. Part II: Direct and indirect components of the response. *J. Climate*, **17 (5)**, 877–889.

Deser, C., R. A. Tomas, and S. Peng, 2007: The transient atmospheric circulation response to North Atlantic SST and sea ice anomalies. *J. Climate*, **20 (18)**, 4751–4767, doi:10.1175/JCLI4278.1.

Dijkstra, H. A., 2007: Characterization of the multiple equilibria regime in a global ocean model. *Tellus*, **59A (5)**, 695–705.

Dokken, T. M., K. H. Nisancioglu, C. Li, D. S. Battisti, and C. Kissel, 2013: Dansgaard-Oeschger cycles: Interactions between ocean and sea ice intrinsic to the Nordic seas. *Paleoceanography*, **28 (3)**, 491–502, doi:10.1002/palo.20042.

Drijfhout, S., E. Gleeson, H. A. Dijkstra, and V. Livina, 2013: Spontaneous abrupt climate change due to an atmospheric blocking–sea-ice–ocean feedback in an unforced climate model simulation. *Proc. Nat. Acad. Sci. USA*, **110 (49)**, 19 713–19 718, doi:10.1073/pnas.1304912110.

Eden, C., and T. Jung, 2001: North Atlantic interdecadal variability: oceanic response to the North Atlantic Oscillation (1865-1997). *J. Climate*, **14 (5)**, 676–691.

Eden, C., and J. Willebrand, 2001: Mechanism of interannual to decadal variability of the North Atlantic circulation. *J. Climate*, **14 (10)**, 2266–2280.

Farneti, R., and G. K. Vallis, 2011: Mechanisms of interdecadal climate variability and the role of ocean–atmosphere coupling. *Clim. Dynam.*, **36 (1-2)**, 289–308, doi:10.1007/s00382-009-0674-9.

Gent, P. R., and Coauthors, 2011: The Community Climate System Model version 4. *J. Climate*, **24 (19)**, 4973–4991, doi:10.1175/2011JCLI4083.1.

Goosse, H., H. Renssen, F. M. Selten, R. J. Haarsma, and J. D. Opsteegh, 2002: Potential causes of abrupt climate events: A numerical study with a three-dimensional climate model. *Geophys. Res. Lett.*, **29 (18)**, 7–1–7–4, doi:10.1029/2002GL014993.

Häkkinen, S., P. B. Rhines, and D. L. Worthen, 2011: Atmospheric blocking and Atlantic multidecadal ocean variability. *Science*, **334 (6056)**, 655–659, doi:10.1126/science.1205683.

Hall, A., and R. J. Stouffer, 2001: An abrupt climate event in a coupled ocean–atmosphere simulation without external forcing. *Nature*, **409 (6817)**, 171–174.

Huber, C., and Coauthors, 2006: Isotope calibrated Greenland temperature record over Marine Isotope Stage 3 and its relation to CH_4. *Earth and Planetary Science Letters*, **243 (4)**, 504–519, doi:10.1016/j.espl.2006.01.002.

Jochum, M., A. Jahn, S. Peacock, D. A. Bailey, J. T. Fasullo, J. Kay, S. Levis, and B. Otto-Bliesner, 2012: True to Milankovitch: Glacial Inception in the new Community Climate System Model. *J. Climate*, **25 (7)**, 2226–2239, doi:10.1175/JCLI-D-11-000.44.1.

Johns, W., T. Shay, J. Bane, and D. Watts, 1995: Gulf Stream structure, transport, and recirculation near 68 W. *Journal of Geophysical Research: Oceans (1978–2012)*, **100 (C1)**, 817–838.

Kageyama, M., and Coauthors, 2013: Climatic impacts of fresh water hosing under Last Glacial Maximum conditions: a multi-model study. *Climate of the Past*, **9 (2)**, 935–953, doi:10.5194/cp-9-935-2013.

Kalnay, E., and Coauthors, 1996: The NCEP/NCAR 40-year reanalysis project. *Bull. Amer. Meteorol. Soc.*, **77 (3)**, 437–471, doi:10.1175/1520-0477.

Landais, A., and Coauthors, 2004: A continuous record of temperature evolution over a sequence of Dansgaard-Oeschger events during Marine Isotopic Stage 4 (76 to 62 kyr BP). *Geophys. Res. Lett.*, **31 (22)**, doi:10.1029/2004GL021193.

Li, C., D. S. Battisti, and C. M. Bitz, 2010: Can North Atlantic Sea Ice Anomalies Account for Dansgaard-Oeschger Climate Signals? *Journal of Climate*, **23 (20)**, 5457–5475.

Li, C., D. S. Battisti, D. P. Schrag, and E. Tziperman, 2005: Abrupt climate shifts in Greenland due to displacements of the sea ice edge. *Geophys. Res. Lett.*, **32 (19)**, L19 702, doi:10.1029/2005GL023492.

Locarnini, R., A. Mishonov, J. Antonov, T. Boyer, H. Garcia, O. Baranova, M. Zweng, and D. Johnson, 2010: World Ocean Atlas 2009, Volume 1: Temperature. S. Levitus, Ed. *NOAA Atlas NESDIS*, **68**.

Manabe, S., and R. J. Stouffer, 1999: Are two modes of thermohaline circulation stable? *Tellus*, **51A (3)**, 400–411.

Martin, T., W. Park, and M. Latif, 2014: Southern Ocean forcing of the North Atlantic at multi-centennial time scales in the Kiel Climate Model. *Deep-Sea Res. II*, doi:10.1016/j.dsr2.2014.01.018.

Merkel, U., M. Prange, and M. Schulz, 2010: ENSO variability and teleconnections during glacial climates. *Quaternary Science Reviews*, **29 (1)**, 86–100, doi:10.1016/j.quascirev.2009.11.006.

Mignot, J., A. Ganopolski, and A. Levermann, 2007: Atlantic subsurface temperatures: Response to a shutdown of the overturning circulation and consequences for its recovery. *Journal of Climate*, **20 (19)**, 4884–4898.

Palmer, T. N., 1993: Extended-range atmospheric prediction and the Lorenz model. *Bull. Amer. Meteorol. Soc.*, **74 (1)**, 49–65.

Pedlosky, J., 1996: *Ocean circulation theory*. Springer, 453 pp.

Pickart, R. S., D. J. Torres, and R. A. Clarke, 2002: Hydrography of the Labrador Sea during active convection. *Journal of Physical Oceanography*, **32 (2)**, 428–457.

Rahmstorf, S., 2002: Ocean circulation and climate during the past 120,000 years. *Nature*, **419 (6903)**, 207–214.

Rasmussen, T. L., and E. Thomsen, 2004: The role of the North Atlantic Drift in the millennial timescale glacial climate fluctuations. *Palaeogeography, Palaeoclimatology, Palaeoecology*, **210 (1)**, 101–116.

Rohling, E., and Coauthors, 2008: New constraints on the timing of sea level fluctuations during early to middle marine isotope stage 3. *Paleoceanography*, **23 (3)**.

Sardeshmukh, P. D., G. P. Compo, and C. Penland, 2000: Changes of probability associated with El Niño. *J. Climate*, **13 (24)**, 4268–4286.

Sardeshmukh, P. D., and B. J. Hoskins, 1988: The generation of global rotational flow by steady idealized tropical divergence. *J. Atmos. Sci.*, **45 (7)**, 1228–1251.

Seager, R., and D. S. Battisti, 2007: Challenges to our understanding of the general circulation: abrupt climate change. *Global Circulation of the Atmosphere*, Princeton Univ. Press, Princeton, N. J., 331–371.

Shields, C. A., D. A. Bailey, G. Danabasoglu, M. Jochum, J. T. Kiehl, S. Levis, and S. Park, 2012: The Low-Resolution CCSM4. *J. Climate*, **25 (12)**, 3993–4014, doi:10.1175/JCLI-D-11-00260.1, [http://journals.ametsoc.org/doi/abs/10.1175/JCLI-D-11-00260.1].

Siddall, M., E. J. Rohling, A. Almogi-Labin, C. Hemleben, D. Meischner, I. Schmelzer, and D. Smeed, 2003: Sea-level fluctuations during the last glacial cycle. *Nature*, **423 (6942)**, 853–858.

Sidorenko, D., and Coauthors, 2014: Towards multi-resolution global climate modeling with ECHAM6-FESOM. Part I: Model formulation and mean climate. *Clim. Dynam., submitted.*

Steffensen, J. P., and Coauthors, 2008: High-resolution Greenland ice core data show abrupt climate change happens in few years. *Science*, **321 (5889)**, 680–684, doi:10.1126/science.1156393.

Stocker, T. F., and S. J. Johnsen, 2003: A minimum thermodynamic model for the bipolar seesaw. *Paleoceanography*, **18 (4)**, 11–1–11–9, doi:10.1029/2003PA000920, [http://www.agu.org/pubs/crossref/2003/2003PA000920.shtml].

Stott, L., C. Poulsen, S. Lund, and R. Thunell, 2002: Super ENSO and global climate oscillations at millennial time scales. *Science*, **297 (5579)**, 222–226, doi:10.1126/science.1071627.

Timmermann, A., S. J. Lorenz, S.-I. An, A. Clement, and S.-P. Xie, 2007: The effect of orbital forcing on the mean climate and variability of the tropical Pacific. *J. Climate*, **20 (16)**, 4147–4159, doi:10.1175/JCLI4240.1.

Ting, M., and P. D. Sardeshmukh, 1993: Factors determining the extratropical response to equatorial diabatic heating anomalies. *J. Atmos. Sci.*, **50 (6)**, 907–918.

Trenberth, K. E., G. W. Branstator, D. Karoly, A. Kumar, N.-C. Lau, and C. Ropelewski, 1998: Progress during TOGA in understanding and modeling global teleconnections associated with tropical sea surface temperatures. *J. Geophys. Res.: Oceans (1978–2012)*, **103 (C7)**, 14 291–14 324.

Tudhope, A. W., and Coauthors, 2001: Variability in the El Niño-Southern Oscillation through a glacial-interglacial cycle. *Science*, **291 (5508)**, 1511–1517, doi:10.1126/science.1057969.

Wunsch, C., 2006: Abrupt climate change: An alternative view. *Quat. Res.*, **65 (2)**, 191–203, doi:10.1016/j.yqres.2005.10.006.

Yeager, S., and G. Danabasoglu, 2014: The origins of late-twentieth-century variations in the large-scale North Atlantic circulation. *J. Climate*, **27 (9)**, 3222–3247, doi:10.1175/JCLI-D-13-00125.1.

Zhang, X., G. Lohmann, G. Knorr, and C. Purcell, 2014: Abrupt glacial climate shifts controlled by ice sheet changes. *Nature*, **512**, 290–294, doi:10.1038/nature13592.

LIST OF TABLES

exp	compset	atmosphere		length [years]	starting year	starting from
		resolution	forcing			
CONT	B	2°	-	1000	-	-
HI	B	1°	-	1300	-	-
LGM	B	1°	-	401	-	-
DO_F	G	2°	-	36	305	CONT
OI_a	G	-	DO_F year 332/333	11	311	HI
OI_b, _c, _d	G	-	DO_F year 312/313	30, 21, 13	299, 311, 321	HI
OI_e, _f	G	-	DO_F year 305/306	13	299, 327	HI, OI_b
DO_a,_b	G	2°	-	102, 90	299, 321	CONT
DO_c,_d	G	2°	-	73, 51	561, 581	CONT
DO_e,_f	G	2°	-	51, 51	401, 899	CONT
DO_X	G	2°	-	198	1001	CONT

TABLE 1. Simulations analyzed and conducted for this study. The letter G and B in column compset refer to ocean-sea ice simulations and the fully coupled version of CESM, respectively. The setup of the different simulations is described in Section 2.

budget term		Labrador Sea			
		year 270 -290	year 310-320	year 320-330	year 381-401
advection	temperature $[Wm^{-2}]$	25.23	23.14	14.95	8.47
	salt$\cdot 10^{-8}$[kg $\cdot$ m (kg $\cdot s)^{-1}$]	10.43	10.45	9.21	7.84
diffusion (incl. convection)	temperature $[Wm^{-2}]$	60	48.54	52.7	9.86
	salt $\cdot 10^{-8}$[kg $\cdot$ m (kg $\cdot s)^{-1}$]	-10.29	-10.33	-9.06	-7.69
surface flux	temperature $[Wm^{-2}]$	-86	-72.45	-69.3	-18.87
	salt$\cdot 10^{-8}$[kg $\cdot$ m (kg $\cdot s)^{-1}$]	-0.15	-0.14	-0.16	-0.15
			year 315-335		
tendency	temperature $[Wm^{-2}]$		-2.2		
	salt$\cdot 10^{-8}$[kg $\cdot$ m (kg $\cdot s)^{-1}$]		-0.016		

TABLE 2. Heat and salinity budget (upper 280 m) of the Labrador Sea (53 $^\circ$ to 65 $^\circ N$ and 60° to 45 $^\circ W$) for the pre-cooling phase (year 270-290) and a phase after the transition (year 381-401). Furthermore two values are given for the transition period (year 310-320 and 320-330). The tendency term is averaged over the transition period. Negative signs imply a cooling and freshening of the box.

LIST OF FIGURES

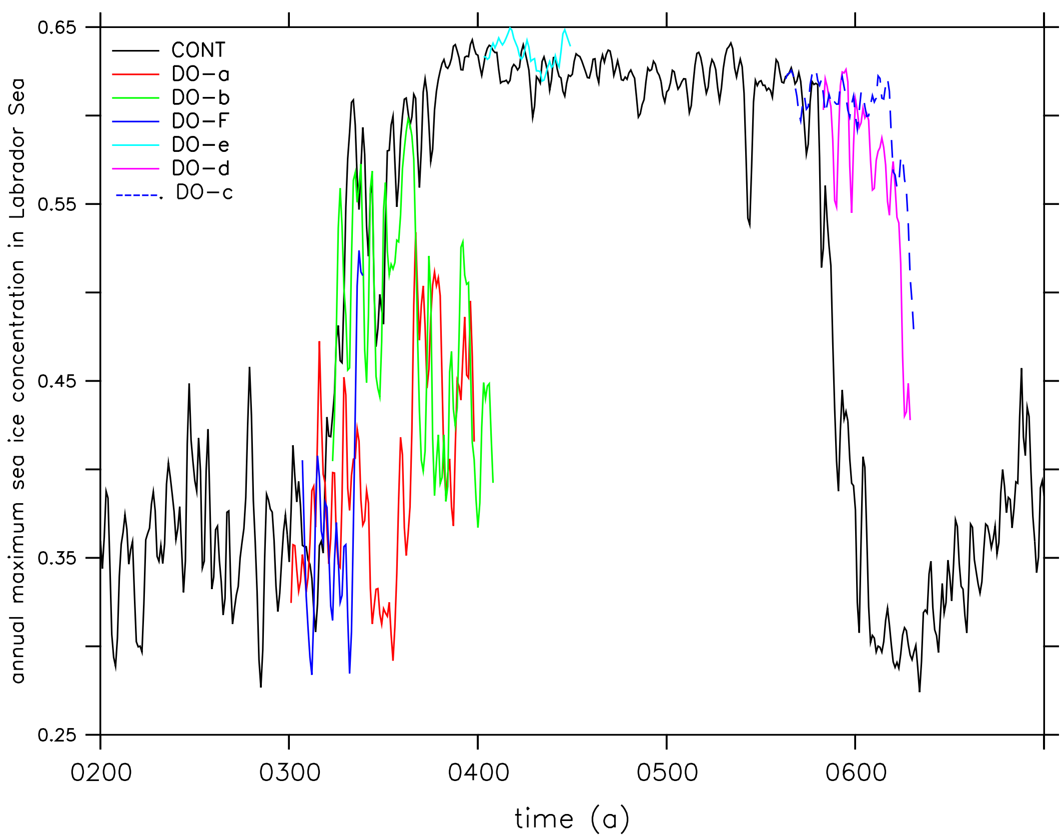

800 FIG. 1. Annual maximum sea ice concentration in the LS (averaged from 65° to 45 ° W and 50° to 70 ° W)
801 for CONT in black, additionally shown are the sea ice concentrations for the different branch runs (different
802 colors), curves are smoothed by a 2 year running mean.

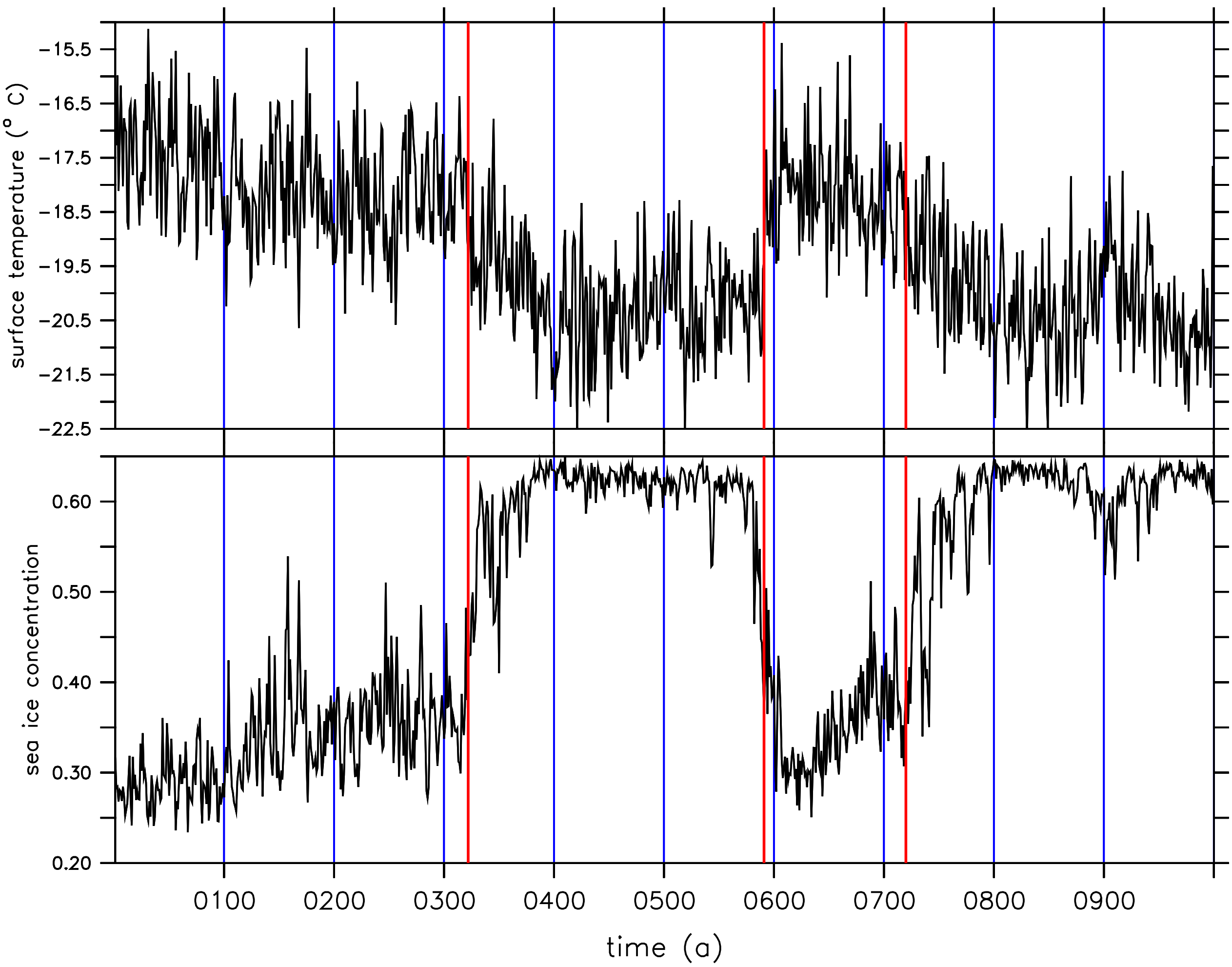

803 FIG. 2. Top: Greenland annual mean surface temperature [°C] averaged from 55 to 15°W and 65 to 80°N (corresponding to Greenland). Bottom: Annual maximum of sea ice concentration in the Labrador Sea (as in Fig. 1).

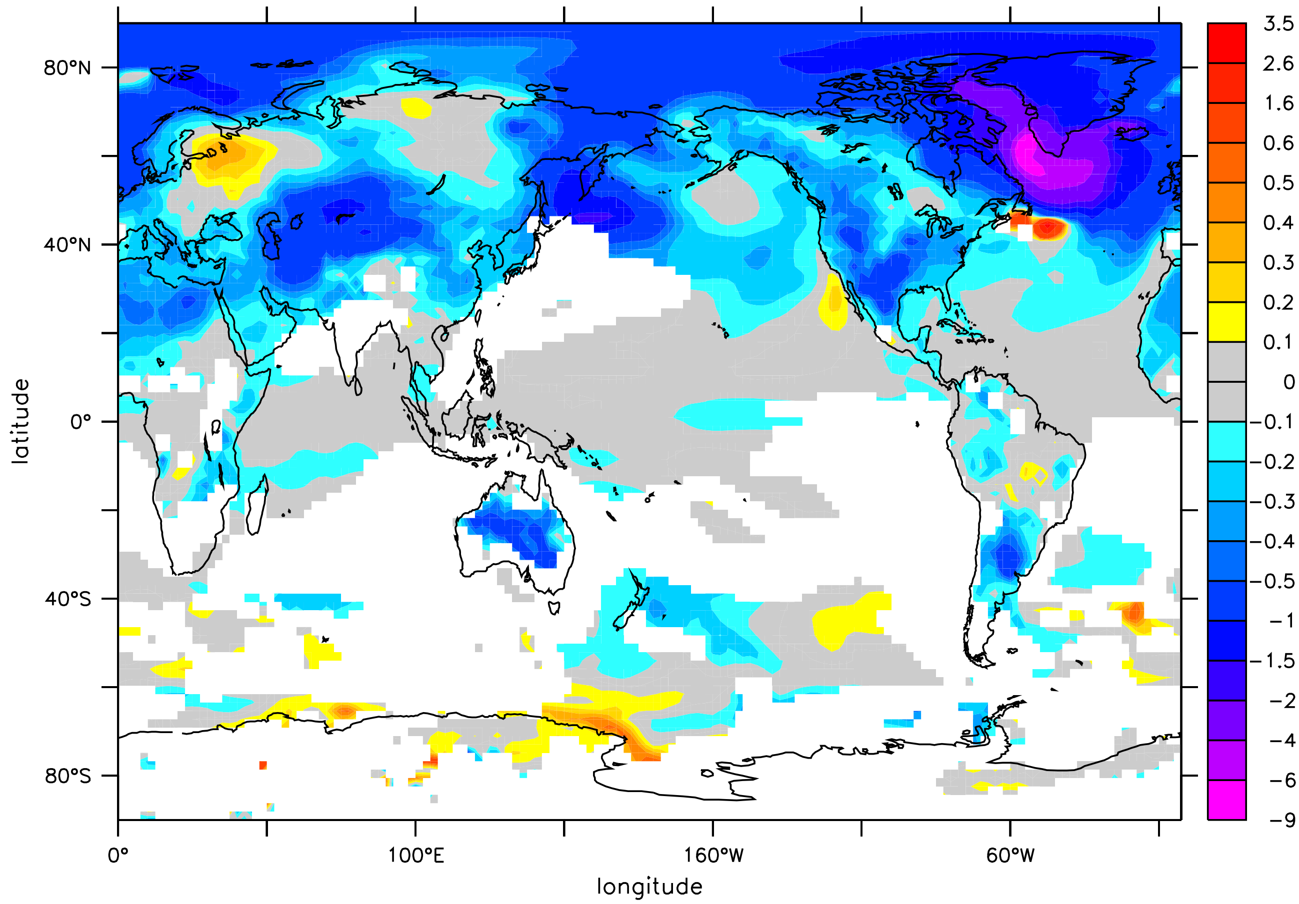

FIG. 3. Global temperature signal: Surface temperature difference between years 350 and 380 (corresponding to the cold NA phase) and 200 and 230 (corresponding to the warm NA phase). Regions are only shaded if correlation with Greenland surface temperature (averaged over the same region as in Fig. 2) for the period between year 250 and 450 is significant on a 95 %-level.

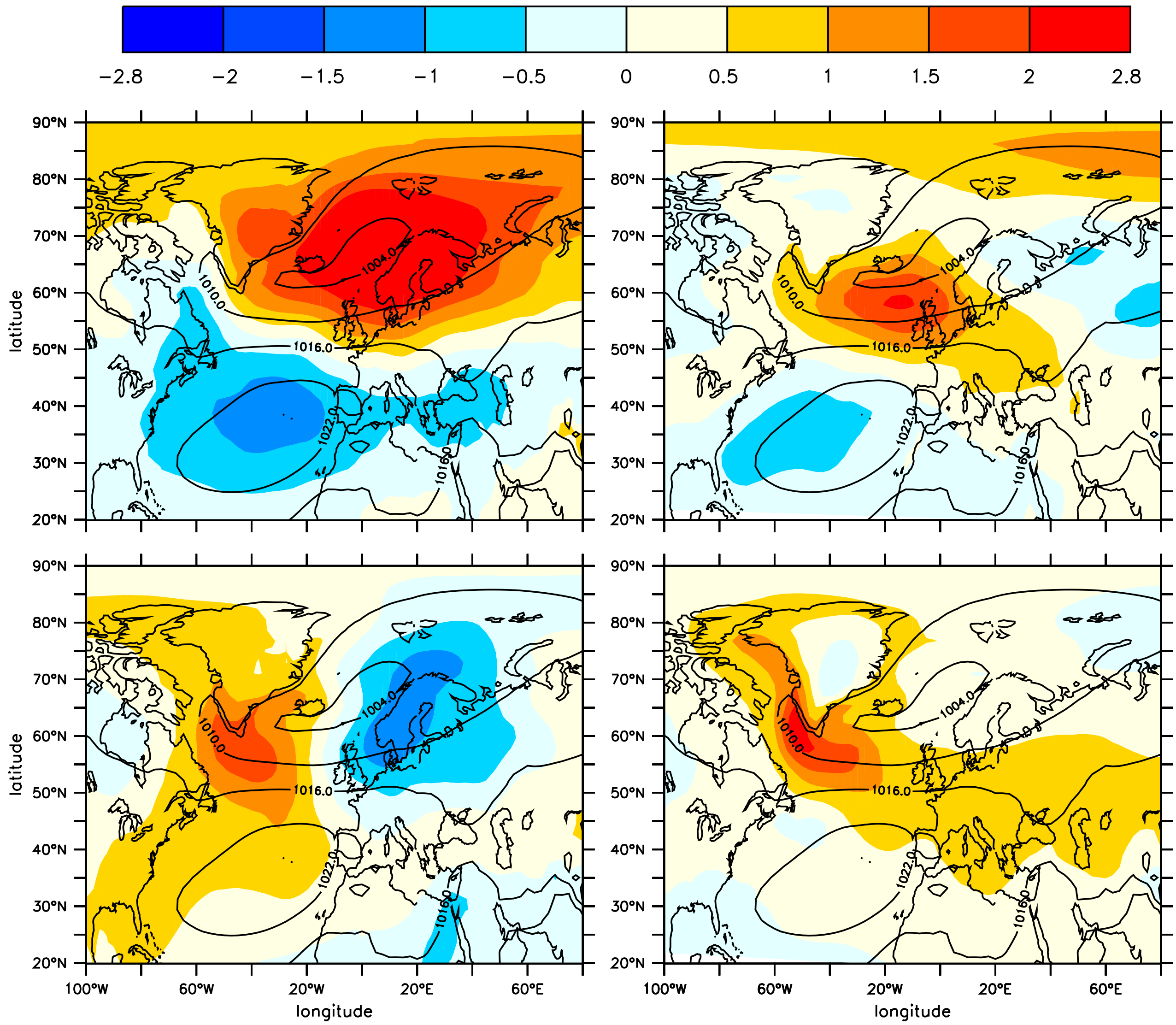

FIG. 4. Sea level pressure anomaly [hPa] for year 310 to 315 (upper left), year 315 to 320 (upper right), year 320 to year 325 (lower left) and for the cold NA phase (year 330 to 580, lower right). All anomalies are relative to the warm phase (year 50 to 250) and positive values imply a higher SLP than during the warm phase. Contours show the 1000 year mean of SLP.

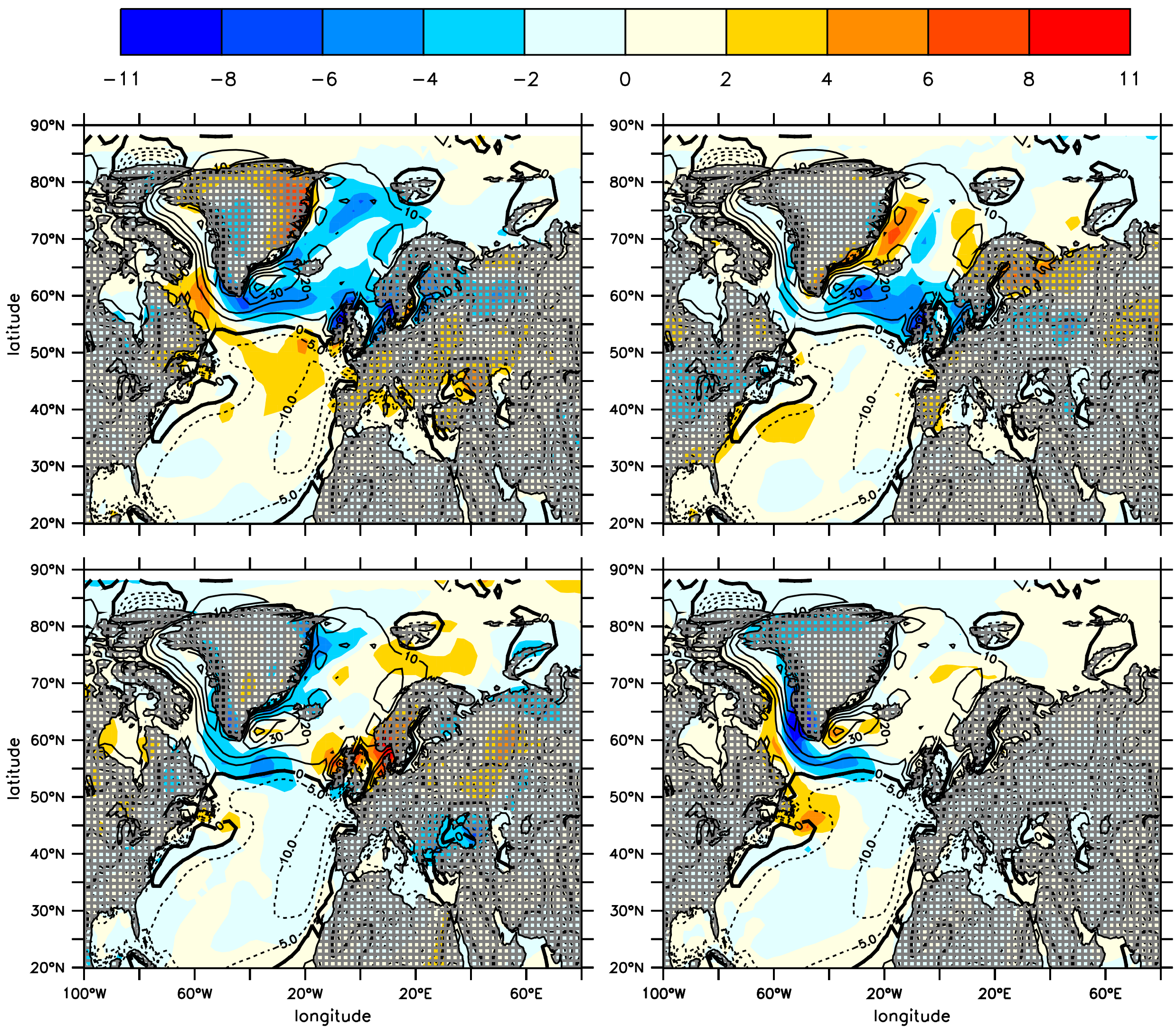

814 FIG. 5. Wind stress curl [$\cdot 10^{-8}$N m^{-3}] for year 310 to 315 (upper left), year 315 to 320 (upper right), year
815 320 to year 325 (lower left) and for the cold NA phase (year 330 to 580, lower right). All anomalies are relative
816 to the warm phase (year 50 to 250). Contours show the the 1000 year mean of wind stress curl.

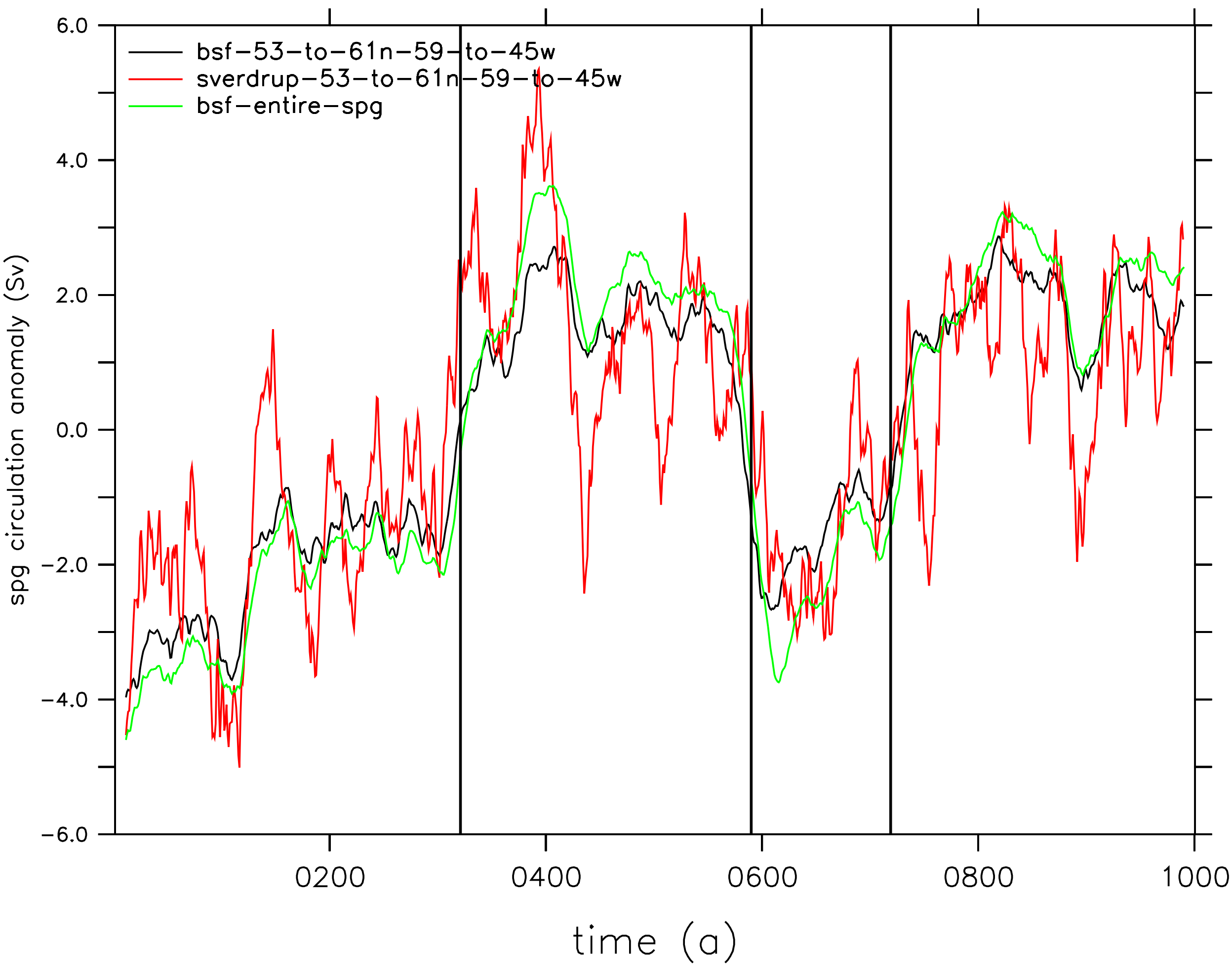

FIG. 6. Sverdrup transport [Sv](red - averaged from 53° to 61°N and 59° to 45°W), actual circulation in the SPG [Sv] averaged over the same region as the Sverdrup transport (black) and over the entire SPG (50° to about 30°W and 43° to 65°N, green). All time series are smoothed by a 20-year running mean.

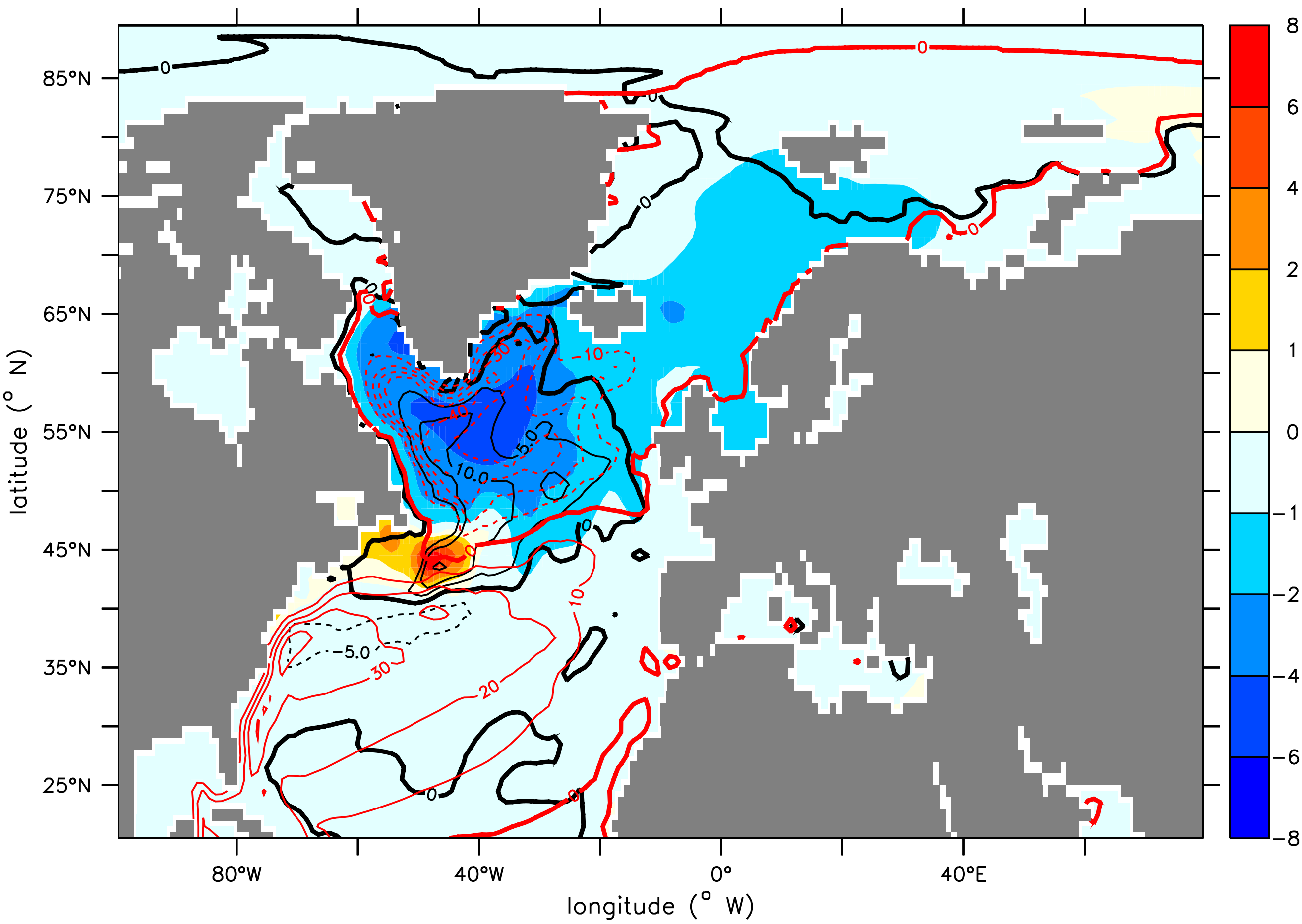

820 FIG. 7. Barotropic stream function anomaly [Sv] (contours) and temperature anomaly [°C] (color) averaged
821 over the upper 100 m in the subpolar gyre, difference between cold (year 350 to 550) and warm (year 50 to 250)
822 NA phase. Contouring interval is 2 Sv, full lines show positive anomalies and dashed lines negative anomalies.

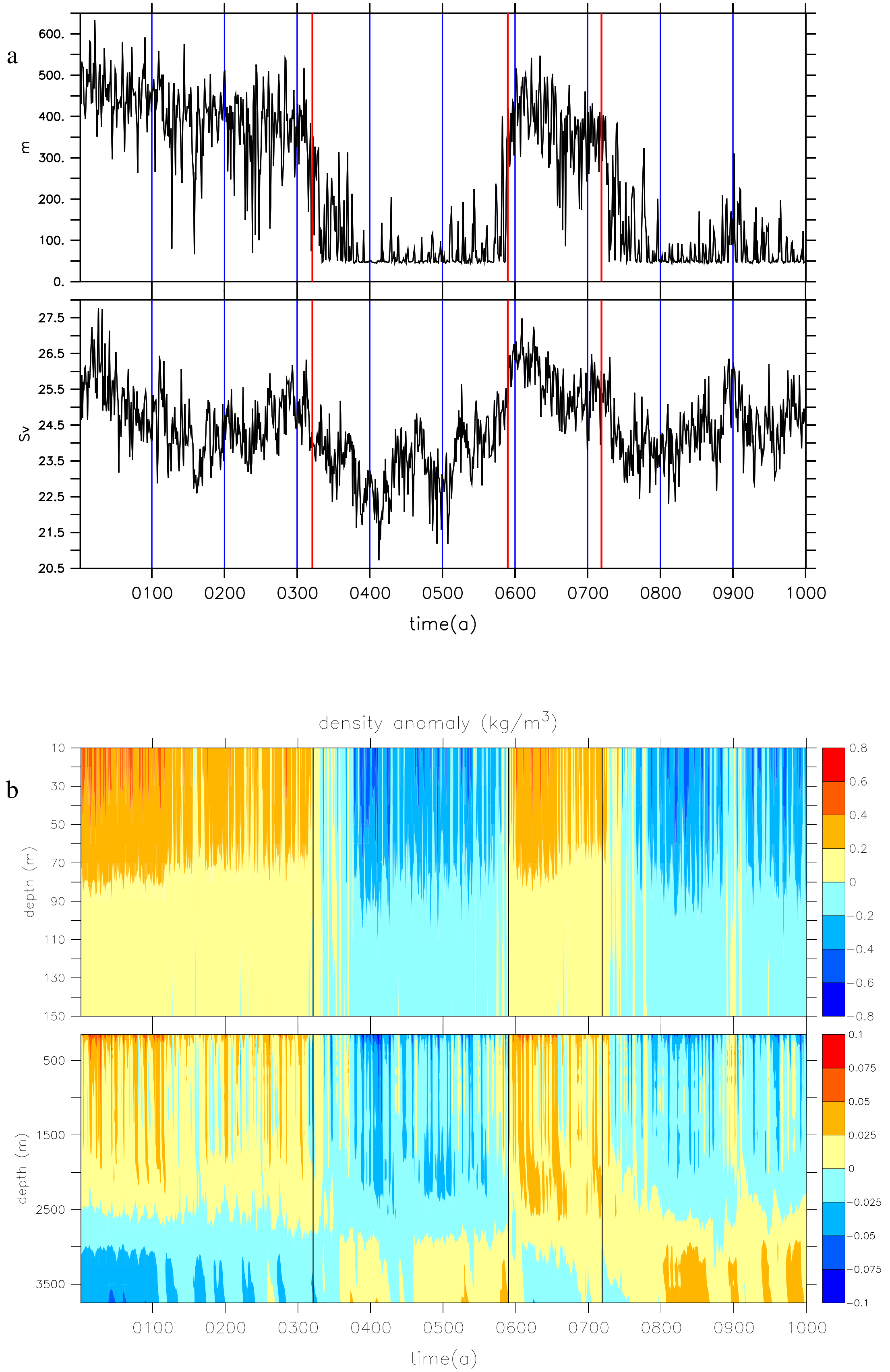

823 FIG. 8. Panel a: MLD in the LS (top, averaged from about 55 ° to 63°N and 60° to 45°W), maximum AMOC
824 (bottom). Panel b: density anomaly in the LS relative to the 1000 year mean. All timeseries are smoothed by a
825 10 year running mean.

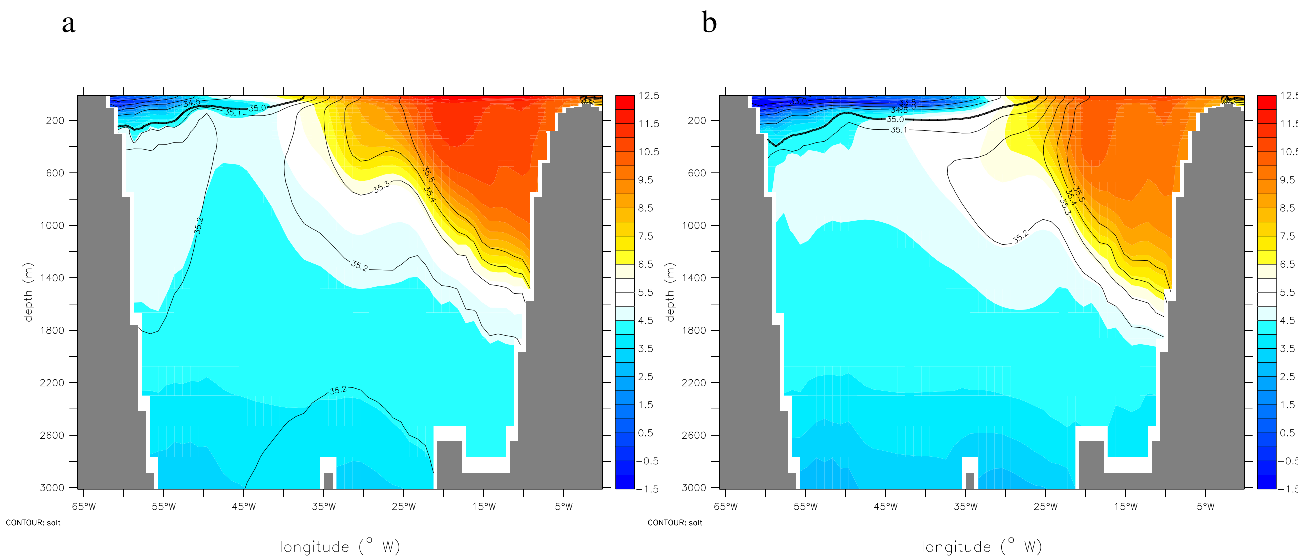

FIG. 9. Temperature (color) and salinity (contours) in a cross section through the SPG averaged from about 54° to 58°N. (a) warm NA phase (year 50 to 250) and (b) cold NA phase (year 350 to 550). Contour intervals are 0.5 psu from 30 to 35 psu and 0.1 from 35 to 35.5 psu.

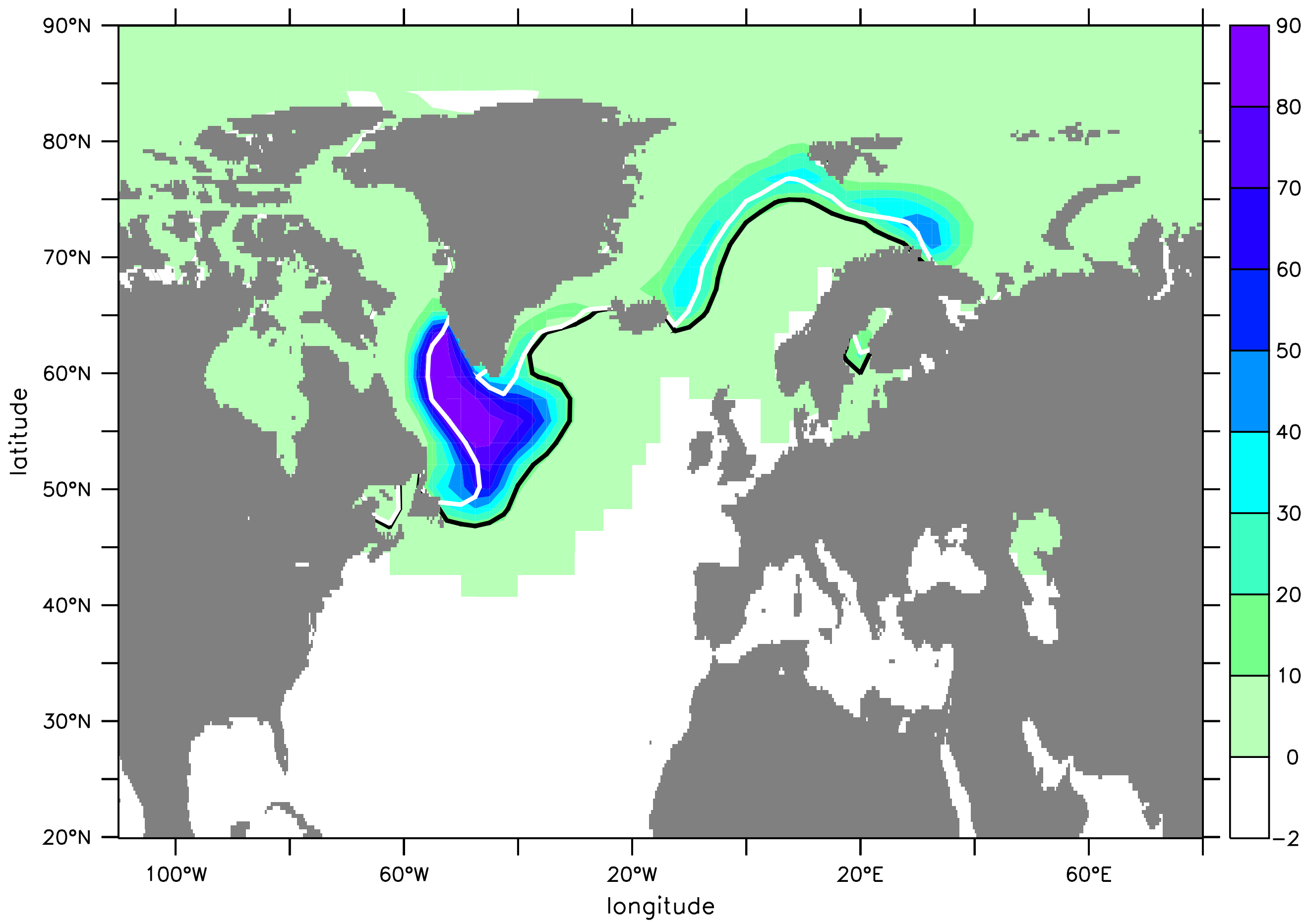

829 FIG. 10. Difference in annual maximum sea ice concentration (in %) between cold phase (model year 380 to
830 550) and warm phase (model year 50 to 250). Overlaying contours show the averaged annual maximum sea ice
831 extent (15%) for the cold phase (black) and the warm phase (white).

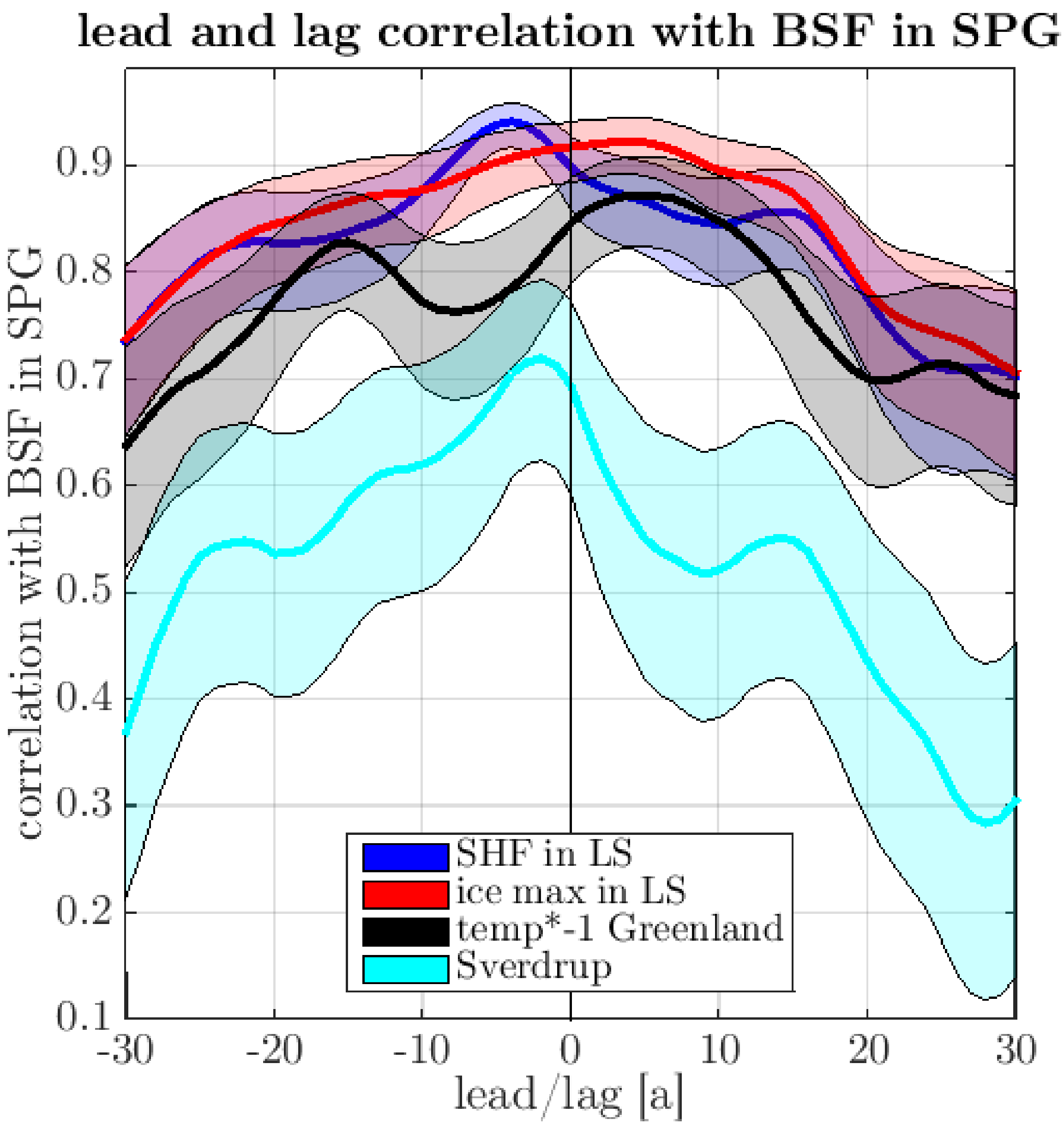

FIG. 11. Correlation for different years of lead and lag of the average BSF in the SPG (same area as in Figure 6) with different variables involved in the climate transition. Surface heat flux in LS (compare to the heat budget in Table 2) in blue. Annual maximum sea ice concentration in the LS (same are as in Figure 2) in red. Greenland temperature (inversed sign; same area as in Figure 2) in black. Sverdrup transport in SPG (same area as in Figure 6) in cyan. Negative years indicate that the variable is leading, while positive years correspond to a lead of the BSF. The correlation is calculated over the timeperiod from year 270 to 400, the data are smoothed by a 5-year running mean beforehand. The shaded areas indicate the 95% interval of the correlation coefficient.

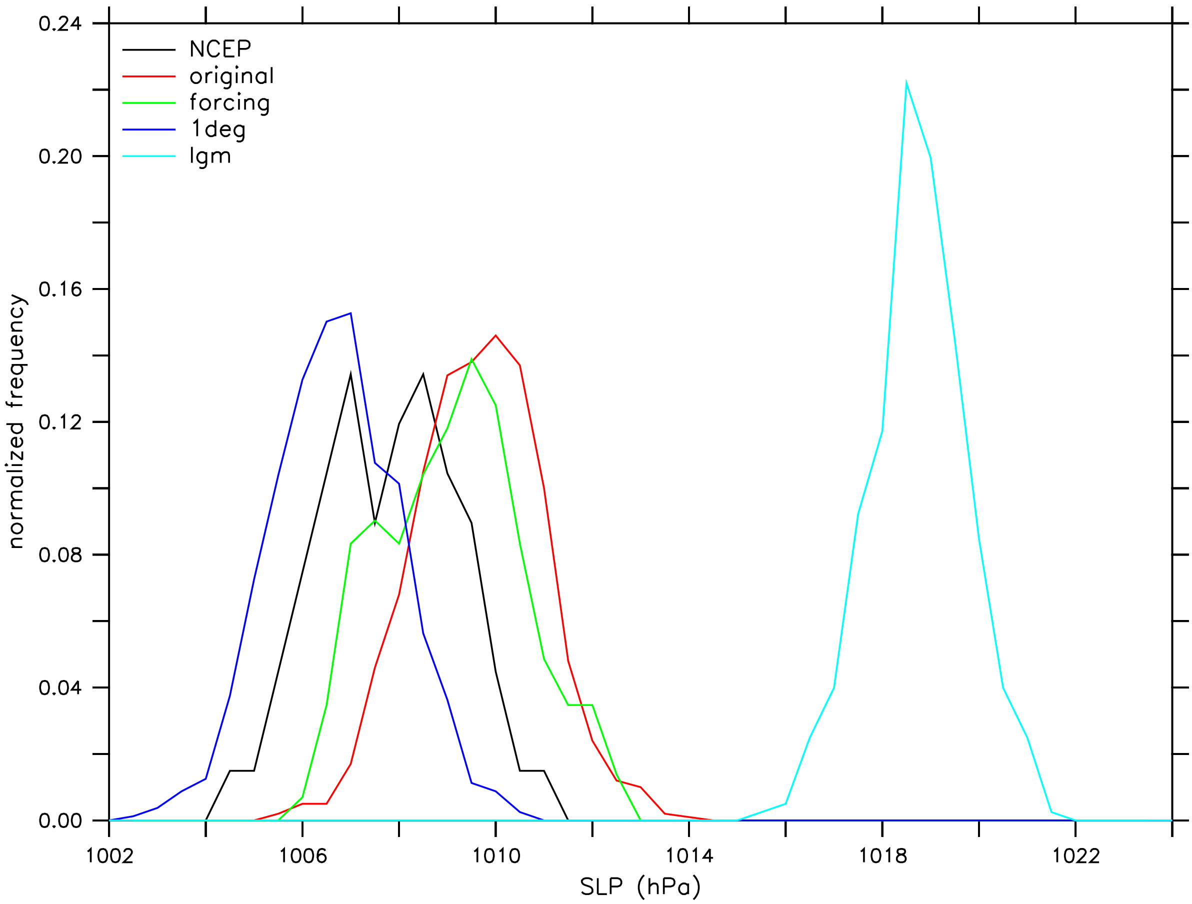

FIG. 12. Comparison of normalised annual SLP [hPa] distribution above the NA (averaged from 50 to 20 $^{\circ}W$ and 50 to 65 $^{\circ}N$) for present-day reanalysis (black), CONT (red), CONT_FORCING (green), HI (blue) and LGM (cyan). Both triggering anomalies of the cold phases have a SLP $>$ 1012 hPa.

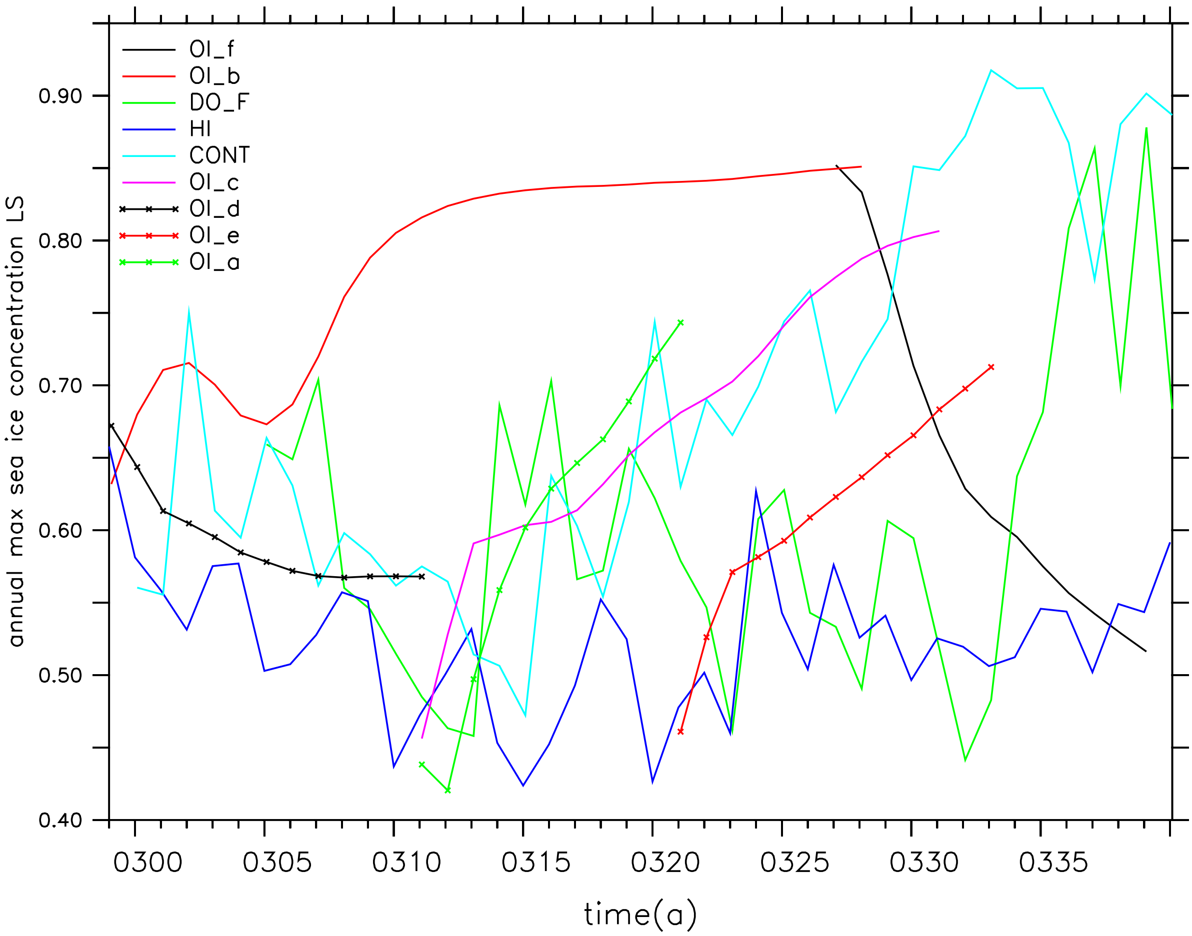

FIG. 13. Annual maximum sea ice concentration in various OI experiments in the Labrador Sea (averaged from about 50° to 67°N and 63° to 40°W), representing the climate transition. Cyan (CONT), blue (HI) and green (DO_F) curves are showing the fully coupled simulations. The remaining curves show the OI experiments, using atmospheric fluxes of year 305/306 (OI_f (black) and OI_d (black with crosses)), year 312/313 (OI_b (red), OI_e (red with crosses) and OI_c (pink)) and year 332/333 (OI_a (green with crosses)) of DO_F as forcing. See Table 1 for experimental setup of simulations.

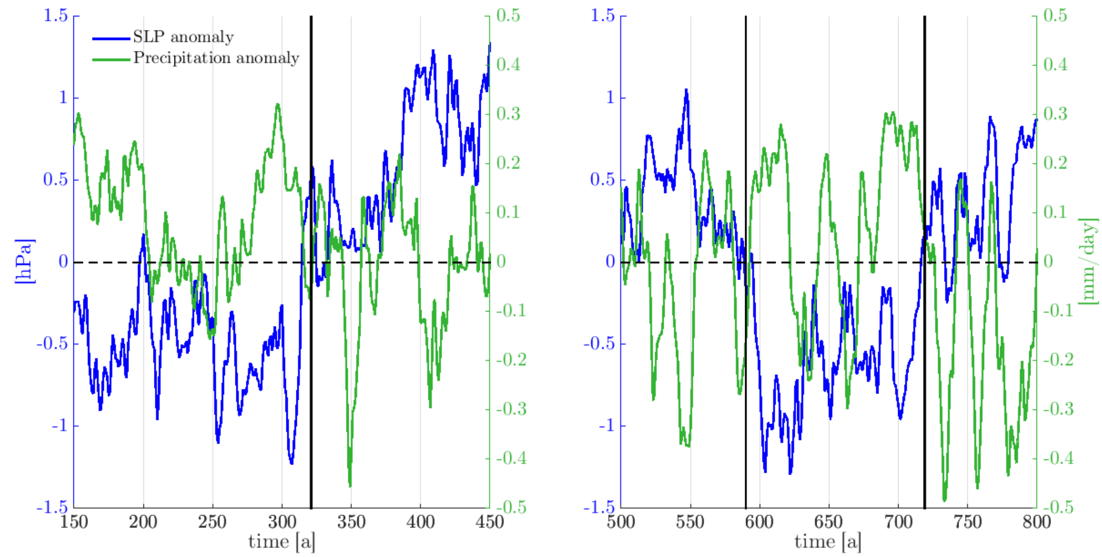

FIG. 14. Precipitation anomaly [$mm \cdot day^{-1}$] in the western tropical Pacific, averaged from 100° to 180 °E and 8°S to 8°N in green and sea level pressure anomaly [hPa] over the NA, averaged from 50° to 20 °W and 50° to 65 °N in blue. Both time series are smoothed with a running mean over 10 years. For the first cooling event around year 310 on the left and for the abrupt warming and the second cooling event around year 600 and 720, respectively on the right.